

Capstone Report - Project NoScope



*Zeyi Lee
Mark Hardiman
Ryan Frazier
Ying Ou
Longxiang Cui
Laura Waller, Ed.
Ming C. Wu, Ed.*

Electrical Engineering and Computer Sciences
University of California at Berkeley

Technical Report No. UCB/EECS-2015-52

<http://www.eecs.berkeley.edu/Pubs/TechRpts/2015/EECS-2015-52.html>

May 9, 2015

Copyright © 2015, by the author(s).
All rights reserved.

Permission to make digital or hard copies of all or part of this work for personal or classroom use is granted without fee provided that copies are not made or distributed for profit or commercial advantage and that copies bear this notice and the full citation on the first page. To copy otherwise, to republish, to post on servers or to redistribute to lists, requires prior specific permission.

University of California, Berkeley College of Engineering

MASTER OF ENGINEERING - SPRING 2015

Electrical Engineering and Computer Science

Signal Processing and Communications

Computational 3D Microscope

ZEYI LEE

This **Masters Project Paper** fulfills the Master of Engineering degree requirement.

Approved by:

1. Capstone Project Advisor:

Signature: _____ Date _____

Print Name/Department: [LAURA WALLER/EECS](#)

2. Faculty Committee Member #2:

Signature: _____ Date _____

Print Name/Department: [MING WU/EECS](#)

ABSTRACT

This project report covers the development of a computational 3D microscope, NoScope. Using tomographic and light field algorithms, we present a method to reconstruct 3D volumes of microscopic samples taken with a lensless sensor. Business and intellectual property strategies for commercializing NoScope are detailed in the first three sections. The remaining sections highlight the project's technical accomplishments and methods.

Capstone Report Project NoScope



Zeyi Lee

A paper submitted in partial fulfillment of the
University of California, Berkeley
requirements of the degree of
Master of Engineering
in
Electrical Engineering and Computer Science

May 2015

Contents

Co-written with Longxiang Cui, Ryan Frazier, Mark Hardiman, and Ying Ou

I Problem Statement

II Capstone Strategy

III IP Strategy

Individually Written

IV Individual Technical Contribution

V Concluding Reflection

Part I

Problem Statement

1 Project Introduction

As technology has advanced with the emergence of digital computing and signal processing, computers that used to take up entire rooms now fit in a backpack, and doctors and nurses have diagnosis equipment built into their cellphones. However, the optical microscope, a piece of equipment crucial for any medical or experimental lab, has remained unchanged for nearly three hundred years. Modern commercial microscopes rely on fragile lenses and precise alignments, and without additional equipment have no means of sharing the acquired images. Heavy and bulky, they are living fossils in a portable world and would benefit greatly from a technological overhaul.

Many fatal diseases, such as malaria, are endemic in tropical areas around the world. In order to better cure people with such diseases, a faster and more affordable detection and diagnosis method is greatly needed in those region. Traditional microscopes had reached their ceiling of being portable due to its fragile nature, and thus cannot be used as a means to diagnose diseases in the field. A more portable device is needed for doctors and nurses working in those area. With a faster diagnose method, millions of lives will be saved every year.

Imagine a world in which the advantages of microscopy are readily available to every individual with a need due to a low price and viability in a wide range of environments. Furthermore, the microscopic images may easily be made digital. Has a boy in a small African village contracted malaria? How can a doctor in a distant area assess over the Internet a patient's health whose disease requires microscopy? These questions find an answer in a robust, inexpensive, and yet powerful digital microscope. Additionally, people everywhere would be free to explore an exciting and useful unseen world.

How can we achieve our vision then? The clue lies in the advent of digitization and higher computational power; we believe these two factors should be the driving force in future of microscopy. Unlike traditional optics, constrained by the limits of the physical world, computational microscopy can ride the tide of improving electronics, compensating for lack of expensive optics with more complex, but more cheaply achievable computations. In particular, the availability of memory and modern processing speed on common consumer devices opens up access to image-processing algorithms that were previously privy to only the world of laboratory work.

As such, our team wishes to leverage the broader trend of digitization to develop a robust, cheap, portable diagnostic tool that can produce digital images of traditional medical samples. With its advanced computational imaging processing technologies, the NoScope manages to create high-resolution digital images without optical lenses. Abandoning the expensive and fragile lenses, NoScope successfully eliminates the high cost and special handle requirement associated with lenses. In addition, since samples are imaged by USB cameras, the digital files can be shared among individuals easily.

Part II

Capstone Strategy

Contents

1	Introduction	1
1.1	Our Product	1
2	Need for Product	4
2.1	Motivating Trends	4
2.2	Satisfying Stakeholders in Medical Diagnosis	5
2.3	Differentiation: NoScope vs Competitors	6
3	Entering the Market	10
3.1	Competitive Forces Analysis	10
3.2	Competitive Pricing in a Saturated Market	15
4	References	18
A	Return of Investment Calculations	22

1 Introduction

By the end of April 2015, the goal of Team NoScope is to produce a minimum viable product of a prototype microscope that creates three-dimensional images of microscopic samples. We plan on accomplishing this through a series of computational algorithms combining principles of limited angle tomography (Kak et al., 1988) and light field imaging (Levoy et al., 1996). Using these imaging techniques, our hardware will create a three-dimensional image from a series of two-dimensional ones. The goal of this paper is to give the reader a brief introduction to our product, then explain its necessity in the market through its key value propositions, and finally elucidate our strategy for entering the congested microscopy market.

1.1 Our Product

The end goal of project NoScope is a fully functioning, robust microscope prototype that can be taken to market as a minimum viable product. The main factors driving our hardware development are portability, durability, and low cost. In order to limit cost, our team has developed a lensless system that bypasses the need for expensive and fragile lenses, which builds upon the LED array illumination technique in Waller Lab (Tian et al., 2014). We have also incorporated a simple microcontroller on the device, allowing the intensive computations to easily be performed by an attached computer. This significantly reduces the number and complexity of parts, when compared to a traditional microscope.

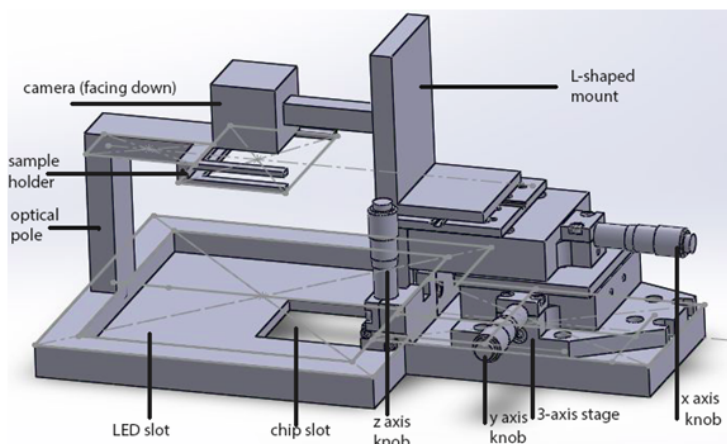


Figure 2.1: Isometric view (CAD) of NoScope.

The current iteration of NoScope consists of a 32x32 matrix of LED's, a camera sensor, and a micro-controller that synchronously triggers specific LED's with camera exposures. During prototyping a custom designed, 3D printed case will house the components. By connecting to a laptop and running software we are developing in parallel with the hardware, the end user will be able place samples on a standard microscope slide and acquire high-resolution 3D images. The inclusion of light field algorithms allows the image to be refocused in post-processing so that various depths of the image can be analyzed by the end user.

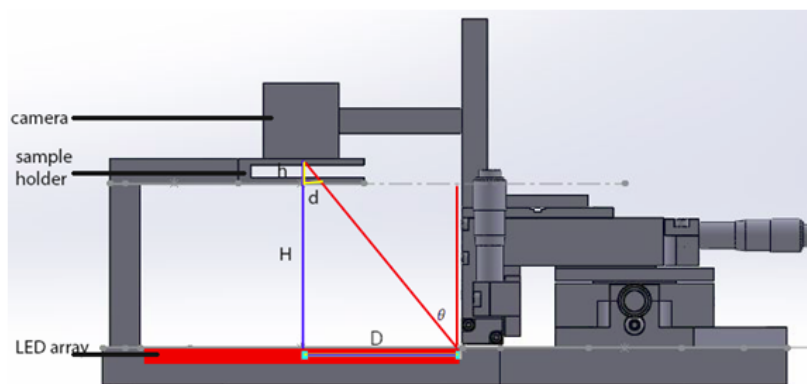


Figure 2.2: Side view hardware schematics of NoScope. Notice the distance of the sample holder to the camera.

Note that figure 2.2 shows the sample placed extremely close (approximately 2mm) away from the camera sensor. This configuration hints at the fundamental working principle of NoScope: casting a shadow of the sample on the sensor. By illuminating a translucent sample, we project an image of the sample on the sensor. Since modern sensors have extremely small pixel pitches (distance between pixel), we are effectively able to view images of its shadow at microscopic scale, thus acting as a microscope. For example, our sensor has a pitch of $5.3\mu\text{m}$.

In addition, we are able to generate different 'views' of the sample by illuminating different LEDs. Since each of the LEDs are placed at a different angle incident to the sample, lighting different LED, and taking separate exposures is analogous to viewing an object at different angles. This also forms the basis for digital refocusing.

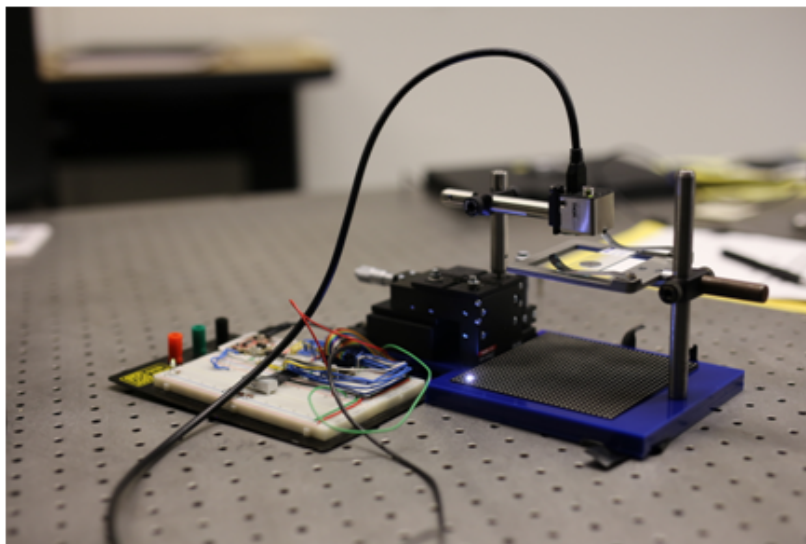


Figure 2.3: First iteration of NoScope. The breadboard is a temporary module and not an actual part of the prototype.

For the current iteration of NoScope, we were able to achieve a resolution of about 32 lp/mm, as well as resolve 3D structures of various microscopic specimens using light field methods. More details can be found in the technical contribution section.

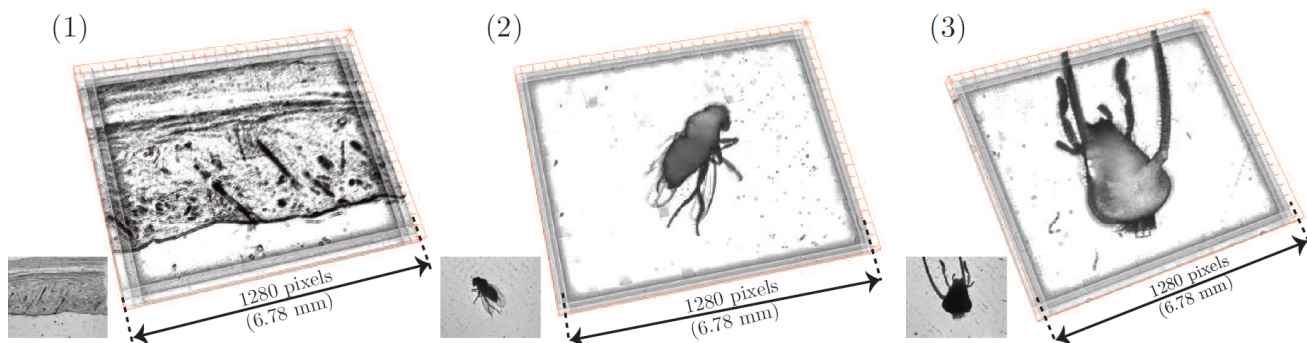


Figure 2.4: Examples of 3D samples from Light field algorithm. No thresholding/post-processing applied. Taken from light field technical contribution report (Lee, 2015).

While the current resolution we can achieve with NoScope is still slightly low, the resolving power of a lensless microscope can be improved by using a sensor with smaller pixel pitch, and better algorithms to account for wave effects. We envision future iterations of NoScope to be used for diagnosing diseases as well as for academic use in teaching environments. In addition, our product can also potentially replace pricey optical microscopes as an inexpensive alternative.

2 Need for Product

Commercialization of NoScope requires the identification of the customers and a full understanding of their needs. In order to find our potential customers, this section will first examine the broader trends in the microscopy industry, and identify a niche for NoScope. Then it narrows down to a specific primary stakeholder and discusses their potential needs, and how these can be fulfilled by NoScope. It further shows that this potential need has not been fulfilled by other products, by analysing the difference between NoScope and our close competitors. Accurate identification of the customer's needs helps companies to shape strategies and have a better positioning. Therefore, this section lays a concrete foundation for our marketing strategy to be discussed in the subsequent section.

2.1 Motivating Trends

As an intrusive new entry, NoScope expects to assist the technology revolution in microscopy and to fulfill needs for underrepresented customers. This section identifies the motivating trends for our microscope in the general industry and our primary market.

Microscopy is a fast growing industry. The market revenue is expected to double in five years from 3.84 billion in 2014 (IndustryARC 2013, p.11). The growing market along with the unique features of NoScope could lead to future investment in NoScope. In addition, this industry is also experiencing a technological shift. The traditional optical microscopes are gradually losing favors due to the limited resolution (IndustryARC 2013, p.13). NoScope might be able to help optical microscopes to regain popularity. The core technology of NoScope is the 4D light field imaging, which is designed to increase the resolution of the sample images without optical lenses. Once this technology has proven to be applicable, it will be possible for NoScope to lead other optical microscope companies to further increase the resolution of optical microscopes.

Despite the industry's maturity, current microscopy still cannot fulfill all its customers' needs. Aside from the expensive cutting-edge equipment being produced by leading companies in this field, there is a significant need for a low-cost product. One particular example is the use of microscopy in malaria diagnosis. According to World Health Organization (WHO), the funding for malaria control and elimination has reached US 2.7 billion by the end of 2013, a threefold increase since 2005, and this

growth of funding has been greatest in Africa Region (WHO 2014, p.12). However, this funding falls far below the 5.1 billion that is required to achieve global targets for malaria control and elimination (WHO 2014, p.12). Replacing expensive microscopes with NoScope can potentially save thousands of dollars for medical facilities, which allows more funding to be channeled into prevention and treatment of malaria.

2.2 Satisfying Stakeholders in Medical Diagnosis

Moving further along the argument of a potential niche in malaria diagnosis, we have thus identified our primary stakeholders as doctors, or medical technicians in malaria-endemic areas. By the end of 2015, there will be about 1 million community health workers in sub-Saharan Africa, estimated by researchers in Columbia University (Singh et al., 2013). However, doctors and nurses alone are not enough to solve the problem. According to WHO, there were about 207 million cases of malaria in 2012 and an estimated 627,000 deaths (WHO 2014b). In order to contribute to the fight against tropical diseases in under-developed regions, we plan to provide these health workers inexpensive and portable microscopes with strong disease diagnosis ability.

The biggest challenge for us is maintaining a low price point. Governments of developing countries cannot afford sufficient expensive medical equipment to satisfy diagnostic needs. On the other hand, doctors from nonprofit organizations mainly rely on donations from external parties, and also have limited budgets. Therefore, expensive microscopes—which are in the range of thousand dollars—are not suitable for our primary customers.

Our key value proposition is thus to make our hardware highly affordable by using a lensless design. Microscopy lenses are particularly expensive, comprising the majority of a typical microscope’s price. Naturally, by avoiding lenses altogether, we can significantly reduce our selling price. This allows our customers to have more money to invest in disease treatment rather than diagnosis.

Our second value proposition is portability and robustness. It is no coincidence that many of the malaria-endemic areas, such as North India, and Africa, are also less economically developed. Consequently, these regions may lack proper transport infrastructures. The conventional microscope lens is a piece of equipment that not only is heavy, but also fragile. As such, these lenses often come with their own protective suitcases. These logistical factors further compound the difficulty of getting

the microscope to the field. By removing the lens entirely, we address the issue of accessibility of microscopic diagnostic services by transforming the microscope into a light, electronic device.

In addition to being lensless, NoScope boasts a unique feature of 3D imaging. The ability to view samples in 3 dimensions can help increase the accuracy of disease diagnosis. Most disease diagnosis relies on morphological discrimination of unhealthy cells based on pathological features (Tadrous, 2011). A 3D image allows doctors to view the sample from different angles, and observe features that might otherwise be hidden in 2D projections or slices. This leads to higher accuracy identification of cell types or parasites. Incidentally, as the following section will show, the 3D imaging feature also distinguishes us from the rest of our competition, making NoScope the most suitable product for disease diagnosis.

2.3 Differentiation: NoScope vs Competitors

In the process of selecting our closest competitors, we have considered the similarity of their technology to ours, as this is a good indication of how directly they compete against NoScope. Building on this, we have further subdivided our competitors coming from the industry and academia. On the commercial side, this section will cover our potential rivals from Lytro, Cellscope, and Pelican. In academia, we will examine the field-portable tomographic microscope by Ozcan Research Group in UCLA.

In comparing our product with those of the competition, we keep in mind the key criteria of cost, portability, and computational imaging capabilities—particularly any 3D capabilities. Although the products of these competitors may hold some advantages over our product in certain areas, NoScope still holds its weight in the market of lightweight, inexpensive imaging systems for disease diagnosis.

Competition in the Industry

In this subsection, we evaluate three industry competitors: Lytro, Cellscope, and Pelican Imaging.

Lytro

We start our industrial competitor analysis from the computational imaging system developed by Lytro. This system is marketed toward everyday users who want to capture depth-related details in their life photos and have more post-processing options available to them to modify these photos. The system boasts a small form factor that makes it convenient to be carried around without hassle. The

light sensor array requires lenses to properly focus the light for capturing light-field information. This light-field technology enables Lytro to vary parameters such as depth-of-field as well as numerical aperture in post-processing (Lytro, 2015), which is a large factor in the appeal of computational imaging systems. However, the method of computational imaging at work in their product does not allow for high-resolution 3D images due to the poor range of angles available to a camera in a macroscopic scene. Most importantly, Lytro does not focus on disease diagnosis and is incapable of microscopy, and thus fills a different need in the imaging market compared with our target customers.

Cellscope

Cellscope offers strictly an optical assembly to accompany a user's smartphone to allow for convenient microscopy while taking advantage of computing power and hardware already in the user's possession. Their product consists of a mount for a smart phone, mirrors and lenses, and a mount for the specimen to be viewed. In concert with a smart phone, this assembly accomplishes the key points of being lightweight and affordable while allowing for taking microscopic images. (Cellscope, 2015) Despite these advantages, Cellscope does not offer computational imaging, and thus has no capability of creating 3D images, which renders it less useful in garnering detailed information about samples, such as malaria parasites.

Pelican Imaging

Pelican Imaging has developed—but has yet to sell or contract out use of—a computational imaging sensor capable of replacing the camera in future smart phone models. The capabilities of a smartphone with this type of integration exhibit much similarity with those of Lytro cameras, particularly post-processing to alter many key characteristics of photos. Hence, we find that Pelican's sensor module matches up against our product in much the same way as Lytro does. However, there is potential for a future product combining Pelican's sensor module as Cellscope to fill the same market need as our product. Such a combination would combine the advantage of 3D imaging with portability and microscopy (Anderson, 2015). However, the optical components present in Cellscope's product may put the price point higher than our product. This combination would also rely on the user to already have a smartphone with Pelican's sensor.

Although this competition is still theoretical at this point, it indicates that there is movement toward filling this niche in the market that we are targeting, and thus informs us to move quickly in developing

our product to gain hold of the market.

Competition in Academia

Field-portable Tomographic Microscope - UCLA

Looking at our academic competitor, Ozcan Research Group in UCLA has a design that bears many similarities to our proposed design. Namely, their microscope employs an LED array, as well as a lensless design, both of which are also key features in our device.

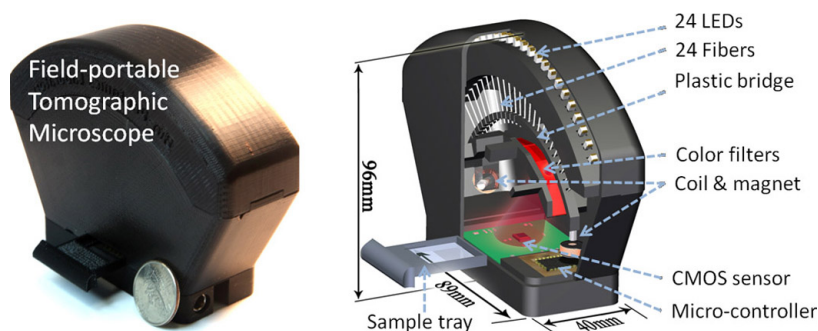


Figure 2.5: The schematics of Ozcan Research Group's tomographic microscope.

[Image Source: <http://www.spie.org/x84293.xml>]

Their image processing technique also resembles ours on the surface. Using multiple angles of illumination, their device takes images of the same specimen at different angles. In addition, in order to extend the angles of illumination beyond one axis, the coil and magnet in the device can electrically actuate the optic fibers to light the sample differently, giving the device an additional axis of data to work with. Following which, the on-board chip on the microscope processes these images into a 3D hologram using the technique of dual-axis tomography (Isikman et al., 2011).

A closer examination reveals several differences between the two devices. In terms of image processing, we are currently tackling the problem using two approaches: 4D light field, as well as 3D tomography. For the more comparable tomography technique, our device differs by virtue of the number of LED axis we have. By employing a full 2D matrix of LEDs, as opposed to just two axes in their device (additional axis by driving coils), our design endows us with multiple axes of data to work with. Consequently, we expect to be able to achieve a higher theoretical fidelity when it comes to reconstructing the 3D structure.

Aside from the algorithm used, we expect our device to be far lower cost than UCLA's microscope, owing to the simplicity of our design. The first reason is that the domed-shaped housing for the LED, which has to be custom made, is much more expensive than a flat piece of LED array we are planning to use, which can be bought off-the-shelf.

Additionally, UCLA's microscope achieves their second axis of illumination by actuating magnetic coils on the device (Isikman et al., 2011). This undeniably adds complexity, and hence cost, to the device. In contrast, as mentioned in the analysis of our tomography algorithm, the nature of our 2D LED array already allows us to have multiple axes of illumination. Taken together, we expect our device to be simpler in design, but still capable of achieving the same, if not better, resolving capability.

From our analysis of competitors above, we find our product provides a service not yet filled by others. Although Lytro, Pelican Imaging, Cellscope and Ozcan's Research group have somewhat similar products, our end goal will serve a need separate from all of them by providing a portable, low-cost microscope capable of 3D imaging focusing on disease diagnosis.

Since we accurately identified the specific need of our stakeholder, we are better able to differentiate ourselves from our competition. As such, we have laid the foundation of a specific need we hope our product will eventually be able to satisfy. The following section will thus use that niche as an anchor to expand on the broader strategy of entering the market.

3 Entering the Market

Successful entrance into our target microscopy market necessitates an overall understanding of the forces and trends permeating this market. In this analysis, we aim to garner insight regarding those technological and business aspects that impact our strategy to enter the market, which include profitability under competitive forces, and the pricing of our product.

3.1 Competitive Forces Analysis

We first seek to gain a thorough understanding of the factors affecting profitability in this market. In evaluating these factors, we apply Michael Porter’s well-known framework of the “Five Forces” model to gauge competitive forces. We further consider positioning ourselves according to Clay Christensen’s “disruptive innovation” model in order to help combat each of these forces.

As this technology has not yet been commercialized in the application of microscopy, considerable opportunity exists in the market for our product. However, we find the current industry environment hostile to new entrants such as ourselves, and we must overcome strong barriers to entry in order to gain a foothold in the market. Substitutes for our chosen application of malaria diagnosis—medical diagnosis and Rapid Diagnostic Test RDT—pose a threat of luring customers away from our product. Finally, we consider what power buyers and supplier might have over our profitability in this market.

Established Rivals

A small number of large companies command most of the power and profit in the microscopy industry; indeed, more than 90% of revenue in the \$5,682 million industry of 2013 went to a limited number of key players (McWilliams, 2013, p. 135). Looking at industry reports, we find that these key players largely consist of glass manufacturers (Uba, 2015, p. 14). The clout of this cluster of glass manufacturers presents a considerable barrier to entry due to the limited number of suppliers. However, since a large advantage of the technology we employ is the lack of optical components such as lenses, we expect to be minimally affected by the clout of this cluster of glass manufacturers. This allows us to circumvent the strong barriers to entry set up by the larger players of the industry.

Established microscope companies have more resources and better reputation than we would upon

entering the market. How then can we penetrate the market to become profitable while minimizing retaliation from incumbents? The answer lies in Clayton Christensen’s “disruptive innovation” model. By taking advantage of the un-catered needs of markets with lower gross margins, we can reach a customer base with a smaller budget and thus enter the market (Christensen, 2015, p. 1). The lensless nature of our system brings our costs low enough to be highly competitive, and undercut the cost of microscopes with similar specifications, as we discuss in the next section on pricing. Large microscope companies will run the risk of degrading their profits in order to compete on a similar price point.

Furthermore, our technology presents its own barrier to mimicry. After searching through commercially available options, we found that computational imaging has not yet been commercialized for any microscope, so companies would be forced to conduct R&D in the field of our technology in order to take advantage of the value that saves product cost. Lastly, even if competitors increase the R&D effort for a comparable product, they run the risk of self-competition. The customer bases between our initial customers and a typical microscope producer are not mutually exclusive; these competitors would compete with their own products for the same customers if they chose to mimic our technology.

Buyers and Suppliers

The buyers of microscopes come from various industries. The life science industry is the largest player on the buyer side with 26% of the market, followed by the semiconductor industry, education, and the nanotechnology industry, with market share as shown in Table 1 below (McWilliams, 2013, p. 7).

Table 2.1: Global microscopes market share by major application, 2012 (McWilliams, 2013, p.7).

Industry	Proportion of Market
Life science	26%
Semiconductors	24%
Education	12%
Nanotechnology	7%

From Table 1, we can clearly see that the life science industry is the biggest player in the buyer’s side, but it does not dominate the market. The semiconductor industry and material science industry both have similar market shares as the life science industry on the buyer side. Furthermore, if we look into

the life science industry, microscopy has been the de facto tool of cell and tissue analysis from 1800 (Rosen, 2005), and it is extremely hard for the industry to find substitutes for the microscope and change its 200 year-old habit. Therefore, we can safely conclude that the buyer power of microscopy industry is relatively weak.

If we look at the components of a microscope, its most expensive and fragile parts are the lenses. Looking at the major supplier microscopes, the optical instrument industry, we find an interesting phenomenon—the major players in the microscopy industry, such as Nikon and Carl Zeiss Ag (McWilliams, 2013, p. 135), also have business in optical instrument manufacturing industry (Oliver, 2015; Uba, 2015). This shows that the suppliers of large microscope companies are themselves; these companies most likely found it profitable to perform backwards integration by bringing manufacturing in-house. The supplier power is thus weak for the large companies in the industry. However, this also means small companies and OEMs in the industry need to buy lens from their major competitors. The supplier power for small companies in the industry is quite high. In order to mitigate the strong supplier power from those big players, we designed our product to be lensless. The electrical components of our product, a LED array and a CCD camera, are easily replaceable. Therefore, we can conclude that the supplier power for our product is also relatively weak.

Threat of Substitutes

Next, we consider the power of substitutes for diagnosis of malaria by evaluating the two major substitutes: clinical diagnosis and Rapid Diagnostic Test (RDT). We show that microscopy remains the de-facto gold standard for diagnosing malaria, and hence, the threat of substitution is weak.

Plasmodium is the malaria-causing parasite. Conventional diagnosis of malaria works by staining a patient's blood smears using a mixture of acidic eosin and methyl blue, known as Giemsa's solution. (Fleischer et al., 2004, p. 2). This solution stains the *Plasmodium* infecting red blood cells, allowing technicians to detect their presence under a microscope.

Unfortunately, the microscope has its limitations; financial and technical obstacles combined preclude microscopy from being more widely used. Current microscopes are inherently bulky and expensive. Furthermore, the typical optical microscope requires a trained technician to operate, increasing the difficulty of getting a good microscopy test in poor rural regions.

In spite of that, medical experts widely consider Giemsa microscopy to be the most reliable method for diagnosis (Murphy et al., 2013, p. 2). This is due to its low per-use cost, at approximately USD \$0.12–0.40 per smear (Wongsrichanalai et al., 2007, p. 6), and its ability to quantify accurately, the severity and variant of *Plasmodium* in the blood sample. This is also the reason why we have targeted malaria diagnosis as our initial market; our simpler lensless microscope can increase the accessibility and affordability of good microscopy service in this much needed market.

Clinical Assessment

We now consider the most basic form of diagnosis: clinical assessment by a doctor. The process of clinical diagnosis starts with recording a patient’s travel history. More specifically, this considers any high-risk endemic area in a one-year window prior to diagnosis, such as Africa, North Korea, or North India. However, this has the flaw of assuming an accurate travel history. In addition, the highly variable incubation period across *Plasmodium* variants means that, in some cases, even a one year period is not enough to cover all bases. For example, the vivax variant of *Plasmodium* found in North India and Korea will only start attacking the body 12-18 months after the mosquito bite (Griffith et al., 2007).

Moreover, even after establishing the travel history, recognizing malaria infection based purely on symptoms is not straightforward. Early symptoms of malaria bear many similarities to other common diseases, such as fever, chills, headache, and malaise. Inevitably, this complication hampers the early diagnosis of malaria, especially when it is at its most treatable stage. Unfortunately, it is only in the later stages in which the most telling, but fatal, symptoms surface. These includes coma, anaemia, hypoglycaemia, and more (WHO, 2010, p. 4).

Ultimately, diagnosis itself cannot provide confirmation of malaria infection. This implies that most clinical diagnosis will invariably fall back on microscopy as a final step. Naturally, it seems reasonable to deduce that pure clinical diagnosis is a weak substitute for giemsa microscopy.

Rapid Diagnostic Test

The next best alternative is known as Rapid Diagnostic Test (RDT). RDTs are dipsticks which indicates the presence of antigens (proteins) secreted by *Plasmodium* in the blood. A patient uses a RDT by pricking a small amount of blood on a test strip containing antibodies targeting specific *Plasmodium* antigens. Depending on the result, the blood colors the test strip in a specific manner, allowing

a quick diagnosis.



Figure 2.6: Example of a Rapid Diagnostic Test, BinaxNOW from Alere. Source: <https://ensur.invmed.com/ensur/broker/ensurbroker.aspx?code=12000304&cs=26232437>

The advantage of using RDT is that it is fast and easy to use. Unlike a microscope, the small RDT test kit can be brought out to the field, and be used by an untrained person by reading off the strip. It also does not require an electricity source. Most importantly, the RDT can give an indication within 5-20 minutes, making it suitable for screening a larger number of people. This also accounts for its recent popularity. These tests are increasing in popularity and use in recent years, with 319 million units of reported sales in 2013, up from 46 million in 2008 (WHO, 2014, p. 22).

Despite its popularity, RDTs remain far from being a microscopy replacement. The first issue is that RDTs are only sensitive towards one variant of *Plasmodium*, the falciparum. For other variants, the RDT becomes less sensitive, especially when parasite density is low (Wongsrichanalai, 2007). This opens up the danger of false negatives. Second, the RDT is unable to distinguish between variants of *Plasmodium*, which is essential for effective treatment. Third, RDTs cannot quantify the concentration of the parasite in the blood, which indicates the severity of infection.

The limitations of RDT put it, at best, a complementary product, rather than a substitute, for microscopy. It is currently well-suited for giving quick diagnosis in areas where microscopes or technicians are unavailable.

Having considered the available substitutes, we believe NoScope attacks a sweet spot in the space of diagnosis by offering diagnostic reliability, accuracy, ease of use (no optical focusing), and affordability. By carefully segmenting an application of microscopy that has no viable substitutes, we have positioned our lensless microscope in a strategically strong position. As such, a vital specification of our microscope is to be able to resolve the *Plasmodium* variants, as well as doing it affordably, in order to

place ourselves in an advantageous position in the malaria diagnosis market.

Upon examining the competitive forces in our chosen market, we expect to encounter strong barriers to entry. We can circumvent profit loss by taking advantage of the lensless nature of our system. This lack of optical components also contributes to our highly competitive price point, which fuels our use of the disruptive innovation model of entering a market. Large companies ultimately would not provide strong retaliation due to factors of price point, R&D costs, and self-competition. We find buyer power weak due to the large demand for microscope and the unique value of NoScope. Supplier power does not dampen profitability considerably due to the interchangeability of suppliers that our system design affords us. Our affordable and powerful design is highly competitive against the available substitutes. Altogether, we expect these competitive forces to weigh little against our potential profitability.

3.2 Competitive Pricing in a Saturated Market

While the previous section covered the broader business strategy, this section will cover our specific competitive pricing tactics for NoScope. Too low of a price will hurt profits and will not allow us to expand quickly. Too high of a price, however, would put us in direct competition with large microscope producers whose brand recognition and R&D power we cannot match.

The Top-down Approach

To determine the optimum price, we used a top down approach and analyzed Nikon's annual shareholder report. As one of the leading microscope producers, Nikon's 2013 net sales for optical instruments was 41.9 million dollars (Nikon, 2013). At an average cost of \$530 per microscope, calculated using <http://amscope.com>'s inventory, this comes to 79,056 units sold per year. Our team wants NoScope to have a 5 year first-generation life cycle with one year of R&D Preceding. Being a smaller startup, our expected sales per year were determined as a fraction of Nikon's annual sales, with expected sales approximately doubling each year as the company grew.

The Bill of Materials for NoScope was calculated using reputable vendors such as DigiKey. This in combination with employee costs was used to calculate annual sunk costs (Figure 2.3). Using this data, we determined that in order to turn a profit on NoScope after three years we would need a product cost of \$120.60. Calculating a 50% buffer for unexpected costs leads to a final price tag of \$189.99 per unit. This is well below the average traditional microscope cost allowing us to compete with

established rivals price-wise, while still remaining competitive in the event of new market entrants.



Figure 2.7: Accumulated costs vs. units sold for product lifecycle

As mentioned above, we estimate NoScope’s Generation 1 Life cycle to last five years. Using the Stages in the Product Life Cycle (Figure 2.4), this would account for our introduction and growth period. While firmware updates will still be pushed through the end of the product’s lifecycle, during the last two years, all hardware development will be shifted towards creating a second generation of NoScope.

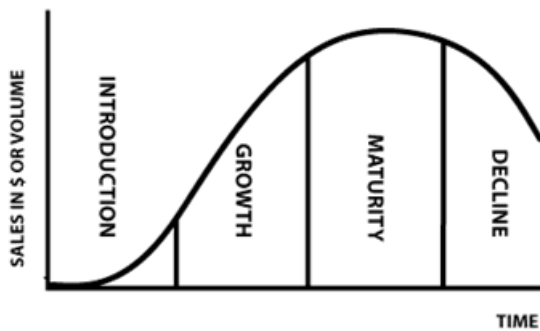


Figure 2.8: Product Life Cycle illustration Source: <https://serrvartisans.files.wordpress.com/2012/03/productlifecycle.gif>

The second generation will be slightly more economical, yet offer more features, such as automatic disease diagnosis and cloud storage services. At this point we will heavily push marketing and brand recognition, having built a stable user base with the first generation model. When NoScope extends from Growth to Maturity, our team will branch off into two distinct consumer products: a medical grade microscope for doctors and other professionals, and a consumer model suitable for schools and

affordable enough to be bought in bulk.

Further on, our company will form an R&D team to research future expansions and applications for our technology. When NoScope enters into the Decline portion of the life cycle, all efforts will be put towards commercializing R&D's prototypes. This may involve changing markets entirely (targeting maker/hobbyist fields instead of medical professionals) and will depend entirely on current market trends. We estimate the total time period from Introduction to Decline to be 10 years, following current market trends as well as the computational "Moore's Law" stating how computing power doubles approximately every 18 months, causing our product to become obsolete if we do not modify it.

4 References

Anderson A.,

Pelican Product, Inc. Hoovers.

<http://subscriber.hoovers.com/H/company360/overview.html?companyId=13868000000000>, Accessed March 1, 2015.

CellScope

2015. Oto Home. https://www.cellscope.com/household/buy_oto_home,

Accessed March 1, 2015.

Christensen, Clay. “Disruptive Innovation.” Clay Christensen. <http://www.claytonchristensen.com/key-concepts/>

Accessed February 16, 2015.

Fleischer B,

2004. Editorial: 100 years ago: Giemsa's solution for staining of plasmodia.

Tropical Medicine International Health 9: 755-756. <http://onlinelibrary.wiley.com/doi/10.1111/j.1365-3156.2004.01278.x/pdf>

Accessed 15 February, 2015.

Griffith KS, Lewis LS, Mali S, Parise ME.

2007, Treatment of Malaria in the United States: A Systematic Review. Journal of American Medical Association.;297(20):2264-2277. doi:10.1001/jama.297.20.2264

http://jama.jamanetwork.com/data/Journals/JAMA/5164/jcr70004_2264_2277.pdf Accessed 15 February, 2015.

IndustryARC

2013. Global Microscopy Devices Market (2013 – 2018) By Types (Electron, Optical & Scanning Probe); By Components (Camera, CMOS Sensors, Display Screen, Lenses, Probe, Scanner, Staining Elements); By Applications (Physics, Chemistry, Forensic Science, Life Sciences, Material Sciences, Semiconductors) <http://industryarc.com/Report/116/microscope-microscopy-devices-market.html>

Isikman, S. O., Bishara, W., Sikora, U., Yaglidere, O., Yeah, J., & Ozcan, A.

2011. Field-portable lensfree tomographic microscope. *Lab on a Chip*, 11(13), 2222-2230.

<http://pubs.rsc.org/en/content/articlepdf/2011/1c/c11c20127a>

Kak, A. C., & Slaney, M.

1988. *Principles of computerized tomographic imaging* (Vol. 33). Siam.

Lytro, Inc

2015. The First Generation Lytro Camera.

<https://store.lytro.com/collections/the-first-generation-lytro-camera> Accessed March 1, 2015.

Levoy, M., & Hanrahan, P.

1996, August. Light field rendering. In *Proceedings of the 23rd annual conference on Computer graphics and interactive techniques* (pp. 31-42). ACM.

<http://doi.acm.org/10.1145/237170.237199>

McWilliams, Andrew

2013. IAS017E - Microscopy: The Global Market. BCC Research. Accessed on 28 February, 2015.

<http://www.bccresearch.com/market-research/instrumentation-and-sensors/microscopes-market-ias017e.html>

Nikon Corporation.

2013. Nikon 2013 Annual Report.

http://www.nikon.com/about/ir/ir_library/ar/pdf/ar2013/13annual_e.pdf

Oliver, Lynett.

“NIKON CORPORATION.” Hoover Company Profile

<http://subscriber.hoovers.com/H/company360/overview.html?companyId=5174200000000>. Accessed February 2015.

Rosen, Shara, Steven Heffner, and LLC Information.

Cell-based Diagnostics: Technologies, Applications, and Markets. New York, N.Y.: Kalorama Information, 2005.

Sean C. Murphy, Joseph P. Shott, Sunil Parikh, Paige Etter, William R. Prescott, and V. Ann Stewart

The Gold Standard: Microscopy, in *Malaria Diagnostics in Clinical Trials*, *American Journal of Tropical Medicine and Hygiene*, 2013 89:824-839; Published online September 23, 2013, doi:10.4269/ajtmh.12-0675

<http://www.ajtmh.org/content/89/5/824.full.pdf+html> Accessed 15 February, 2015.

Singh, P., Sachs, J.D.

2013. 1 million community health workers in sub-Saharan Africa by 2015.

http://1millionhealthworkers.org/files/2013/01/1mCHW_article_Lancet_2013-03-29.pdf

Tadrous, P.J.

2011. Subcellular Microanatomy by 3D Deconvolution Brightfield Microscopy: Method and Analysis Using Human Chromatin in the Interphase Nucleus. *Anatomy Research International*, 28(7), 501503.

<http://www.hindawi.com/journals/ari/2012/848707/>

Tian, L., Wang, J., & Waller, L.

2014 .3D differential phase-contrast microscopy with computational illumination using an LED array. *Optics Letters*, 39(5), 13261329. 2014 March

<http://ol.osa.org/abstract.cfm?URI=ol-39-5-1326>

Uba, Tracy.

2015. "Carl Zeiss AG." Hoover Company Profile

<http://subscriber.hoovers.com/H/company360/overview.html?companyId=59002000000000>. Accessed February 10, 2015.

Ulama, Darryle

2014. IBISWorld Industry Report 33441a: Semiconductor & Circuit Manufacturing in the US. <http://www.ibis.com>, Accessed February 16, 2015.

Wongsrichanalai, Chansuda, Mazie J. Barcus, Sinuon Muth, Awalludin Sutamihardja, and Walther H. Wernsdorfer.

2007. "A review of malaria diagnostic tools: microscopy and rapid diagnostic test (RDT)." *The American journal of tropical medicine and hygiene* 77, no. 6 Suppl : 119-127.

http://www.ajtmh.org/content/77/6_Suppl/119.full.pdf+html Accessed 15 February, 2015.

World Health Organization (WHO)

2010: Clinical Disease and Epidemiology: Guidelines for the Treatment of Malaria, Second Edition

http://whqlibdoc.who.int/publications/2010/9789241547925_eng.pdf Accessed 15 February, 2015

World Health Organization

2014. World Malaria Report 2014.

http://www.who.int/malaria/publications/world_malaria_report_2014/en/ Accessed February 16, 2015.

World Health Organization

2014b. Malaria Fact Sheet in WHO Media Centre

<http://www.who.int/mediacentre/factsheets/fs094/en/> Accessed February 16, 2015.

A Return of Investment Calculations

Costs Calculation

	Year 1	Year 2	Year 3	Year 4	Year 5	Year 6
41900000	0	0	7876	23628	55132	118139
Annual Sales:	0	0	0.1	0.3	0.7	1.5
						236278
						3

Part #	Units per Part	Cost Per Part	Annual Cost	
ATtiny2313	1	0.745	\$5,867.58	
HC595 Shift Reg	1	0.1108	\$872.65	
LED Matrix	1	50	\$393,796.99	
CMOS Camera	1	2.02	\$15,909.40	
Camera Module	1	20	\$157,518.80	
Housing	1	10	\$78,759.40	\$652,724.82

Part #	Units per Part	Cost Per Part	Annual Cost	
ATtiny2313	1	0.745	\$17,602.73	
HC595 Shift Reg	1		\$0.00	
LED Matrix	1	50	\$1,181,390.98	
CMOS Camera	1	2.02	\$47,728.20	
Camera Module	1	20	\$472,556.39	
Housing	1	10	\$236,278.20	\$1,955,556.48

Part #	Units per Part	Cost Per Part	Annual Cost	
ATtiny2313	1	0.745	\$41,073.03	
HC595 Shift Reg	1		\$0.00	
LED Matrix	1	50	\$2,756,578.95	
CMOS Camera	1	2.02	\$111,365.79	
Camera Module	1	20	\$1,102,631.58	
Housing	1	8	\$441,052.63	\$4,452,701.97

Part #	Units per Part	Cost Per Part	Annual Cost	
ATtiny2313	1	0.745	\$88,013.63	
HC595 Shift Reg	1		\$0.00	
LED Matrix	1	20	\$2,362,781.95	
CMOS Camera	1	2.02	\$238,640.98	
Camera Module	1	15	\$1,772,086.47	
Housing	1	8	\$945,112.78	\$5,406,635.81

Costs Calculation

Part #	Units per Part	Cost Per Part	Annual Cost	
ATtiny2313	1	0.745	\$176,027.26	
HC595 Shift Reg	1		\$0.00	
LED Matrix	1	20	\$4,725,563.91	
CMOS Camera	1	2.02	\$477,281.95	
Camera Module	1	15	\$3,544,172.93	
Housing	1	8	\$1,890,225.56	\$10,813,271.62

Employee Costs	Engineers	Executives	Support Staff	Support Payroll
Year 1	5	0	0	\$500,000.00
Year 2	3	2	2	\$700,000.00
Year 3	6	2	3	\$1,050,000.00
Year 4	6	2	5	\$1,150,000.00
Year 5	8	2	7	\$1,450,000.00
Year 6	13	2	10	\$2,100,000.00

		ROI					
ROI Period (yrs)	3						
Year	1	2	3	4	5	6	
Total Costs:	\$500,000.00	\$1,352,724.82	\$3,005,556.48	\$5,602,701.97	\$6,856,635.81	\$12,913,271.62	
Product Cost:	\$120.75						
Product Cost (x1.5)	\$181.12						

Part III

IP Strategy

1 Introduction

This portion of the report is not meant to be an exhaustive analysis on all possible forms of intellectual property protections. Instead, this is meant to be an extension on our business strategy in the previous section, and a brief outlook on the most pressing IP concerns that may aid or hamper us in NoScope's competitiveness in the microscopy arena.

The most unique and potentially patentable portion of our project is the hardware. Four main pieces comprise our system: the LED array and its controlling system, a sample holder, a camera sensor, and a moving stage to mount the sensor. In particular, it is the specific combination of these components that succinctly captures the three critical value propositions of our project: 3D imaging, lack of lenses, and super-resolution. Light from different, single LEDs will cast shifted images of a specimen directly on our CCD camera sensor, giving us the angular information we need to perform 3D reconstruction of the specimen. In addition, the moving stage allows us to translate the camera sensor in microscopic scales - this creates multiple shifted versions of a single image, allowing us to combine these images using super-resolution techniques to a higher resolution than our physical pixel would allow.

The reasons to focus on hardware patenting over image processing algorithms stem from concerns of practicality. First, most of the algorithms we use are based on already published work, precluding any sort of claim on them. Second, many of our competitors have successfully patented their hardware, and this sets a strong precedence for us to consider following the same route. Moreover, one of our close academic competitors from UCLA, which we have analyzed in the business strategy paper, has successfully patented a utility patent with USTPO.

However, the fact that the UCLA Ozcan group has filed a patent using a technology very similar to ours is also a cause of concern. In the next section, we will examine in detail, their group's patent, and demonstrate that our hardware does not infringe their claim. Finally, after establishing the viability of obtaining a patent, we will explain why team NoScope believes that, although obtaining a patent is crucial for getting the product to market, it will do little to maintain our competitive edge in the long-term.

2 Examining our Competitor’s Patent

The name of the patent is “Lens-free wide-field super-resolution imaging device”. Its schematic representation of the invention is shown in figure 1 below. In the abstract of the patent, the group describes their design as an imaging system with “an image sensor and a sample holder disposed adjacent to the image sensor” (Ozcan et al, 2014), which bears similarity to our design. Their design also includes “an illumination source configured to scan in two or three dimensions relative to sensor array” (Ozcan et al, 2014), which is also similar to our system. They included LEDs as one type of their illumination sources. In addition, they mentioned in the patent “the system includes least one processor configured to reconstruct an image of sample”, similar to NoScope.

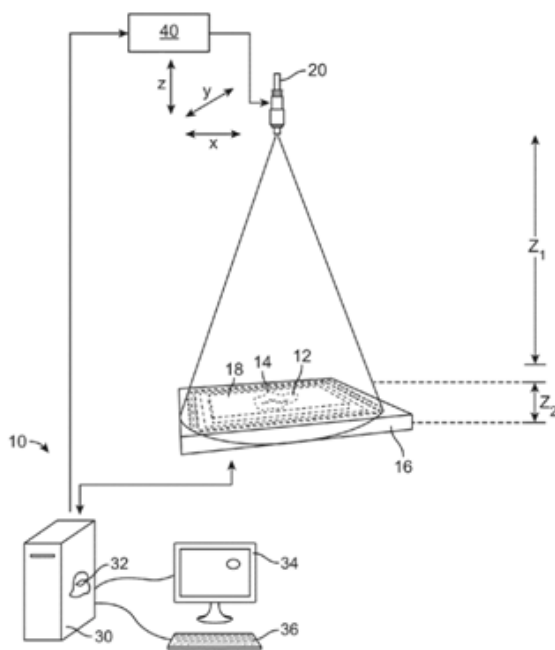


Figure 3.1: Schematic representation of invention of patent filed by Ozcan Research Group (Ozcan 2014, p3)

2.1 Their Five Claims

Although Ozcan’s patent has many similarities to our own, there is no possibility of a successful lawsuit on their part due to key distinctions between their patent’s claims and our product. Ozcan’s patent has 29 claims (Ozcan et al, 2014), which serve to distinguish whether infringement has occurred. Of these 29 claims, there are five main ones with the rest being smaller elaborations to the “big five”

claims, e.g., different light sources or minor changes to the setup. The major claims are diagrammed below.

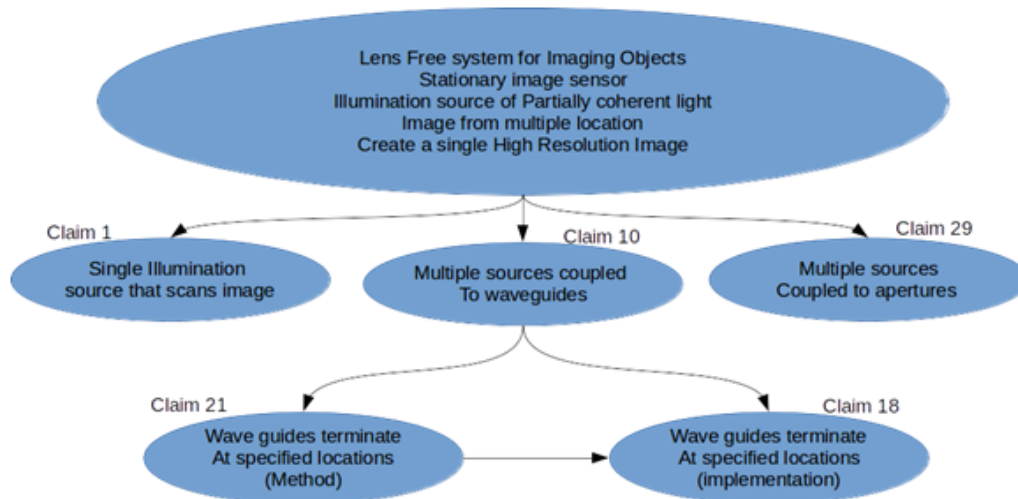


Figure 3.2: Summary of 5 major claims of Ozcan’s lens-free microscope.(Ozcan 2014). Arrows connecting claims imply that the claim has all the features of its parent claim, and additionally its own sub-features.

To analyze whether our group would be in violation of these claims, each major claim was analyzed using the concept of “Doctrine of Equivalents”, articulated in a classic Warner vs. Hilton law case as a test for whether a product violated the claims of a patent (Warner/Hilton, 1997). The Doctrine acts as a three point test. If a product “performs substantially the same function in substantially the same way to obtain the same result,” (Warner/Hilton, 1997) it is in violation of the patent’s claim. Fortunately for our group, while parts of Ozcan’s claims perform substantially the same function in substantially the same way, none of them obtain the same result. Ozcan’s patent exclusively covers the creation of a single high-resolution, or “super-resolution” image from a series of lower resolution images. Our group creates a 3D image of the object being imaged, and does not currently make any claims for super-resolution imaging, as we are limited by the resolution of our imaging device. This notable difference would make us exempt from any infringement claims Ozcan’s group could make regarding their patent.

3 Competitive Advantage of a Patent

In our previous section, we examined one of our closest academic competitors, Ozcan Group of UCLA, and determined that it is indeed possible for us to file a similar hardware patent that would not infringe on any of their claims. In this section, we will examine the competitive advantages a patent confers in getting our product to market, and finally, make an overall recommendation on devising our intellectual property strategy.

3.1 Differentiation - Hallmark of Innovation

A key advantage of filing for a patent is that it acts as a key differentiating point for our product, especially in a technologically driven industry like microscopy. According to BCC, which performed a filtered search for on USPTO, a large company such as Olympus holds approximately 58 utility patents on optical microscopy (McWilliams 2013: 38). In pitting against ourselves against these large rivals in microscopy, a patent is almost a necessity in signifying technological innovation in our product.

In addition, patents are also vital for the process of raising capital if we were to begin as a startup company. For a startup with focus on selling a hardware device, a patent is not only a direct indication of innovation, it is also the assurance that we hold the legal right to produce and manufacture the product. Conversely, a lack of patent raises doubts from potential angels or venture capitalists looking to invest into NoScope. Obtaining a patent would be an unavoidable requirement if we wish to start a company around our lensless microscope.

3.2 Looking beyond the patent

However, beyond the practical purpose of securing funding and differentiating ourselves from our competitors, a patent will provide negligible long-term competitive advantage in the microscopy market. The first reason is that microscopy is by nature an international market. Filing for patent protection in multiple countries is both time-consuming and expensive. In traditional optical microscopes, the U.S. only accounts for 34% of the overall market (McWilliams 2013: 125). Moreover, as detailed in our strategy section, we are targeting malaria-endemic areas, which includes a considerable number of countries such as North India, and regions in Africa. Unfortunately, IP laws are only applicable in the country in which the patent is filed. Our lensless design will not be protected in our primary geographical market, and the financial resources required for multiple patent filings is prohibitive for

a new entrant like us.

Moreover, unlike what conventional wisdom would suggest, a patent in the microscopy market is unlikely to prevent competitors from producing similar, yet non-infringing designs. For imaging in microscopy, multiple ways of achieving the same function exist, many of which are based on well-established academic work, such as super-resolution. A clear example would be how we ourselves have circumvented UCLA's patent claims with a different illumination device, as well as using a moving sensor stage, in order to achieve similar functions of pixel super-resolution. Thus, it does seem reasonable to deduce that there will likely be potential competitors producing altered designs that can directly compete with NoScope.

Taking into consideration the above drawbacks, our group thus believes that obtaining a patent is a necessary step in order to bring the product to market. While it is necessary for raising capital in the early stages, a patent will not help us establish a monopoly in the malaria niche we segmented. This brings us back to our final point we made in our business strategy paper: a long term sustainable advantage in the microscopy market requires constant innovation, and a continually improving product.

Part IV

Individual Technical Contribution

Light Field Methods and Super-resolution

Abstract

This technical report summarizes my contribution in light-field and super-resolution algorithm for NoScope. The first section delves on various methods of 2D digital refocusing – the refocused 2D stack as a foundation for 3D reconstruction. Following which, I implemented and evaluated two different 3D reconstruction method, 3D deconvolution and focus extraction. Finally, the report moves on to the implementation pixel super-resolution algorithms. With the NoScope setup, I was successfully able to achieve 4x super-resolution using the Papoulis-Gerchberg method.

Contents

1	Introduction	1
2	Light Field Methods	2
2.1	Digital Refocusing using 4D Light Field	3
2.1.1	Methodology – Shift-Add Implementation on Lensless setup	3
2.1.2	Results and Discussion	5
2.2	Localized Focusing	7
2.2.1	Methodology – Local Registration	7
2.2.2	Results and Discussion	7
3	3D Reconstruction	10
3.1	3D Deconvolution	10
3.1.1	Projection Model and Lucy-Richardson Algorithm	11
3.1.2	Methodology	13
3.1.3	Results and Discussion	13
3.2	An Novel Alternative: Hacking the 3D reconstruction	15
3.2.1	Methodology – Focus Estimation and Extraction	16
3.2.2	Implementation and Discussion	17
3.2.3	Comparison with 3D Deconvolution	18
4	Pixel Super-resolution	19
4.1	Methodology - Papoulis-Gerchberg Algorithm	20
4.1.1	Results and Discussion	21
5	Conclusion	24
	References	25

List of Figures

- 4.1 Capturing angular data via sequential LED lighting. 3
- 4.2 Principle of digital refocusing. 4
- 4.3 Sample results from digital refocusing. 5
- 4.4 Sample results from local registration refocusing. 8

- 4.5 Results of 3D deconvolution on simulation. 14
- 4.6 Results of 3D deconvolution on actual samples. 15
- 4.7 Focus extraction process flowchart. 16
- 4.8 Results of 3D reconstruction from focus extraction. 17

- 4.9 Results and comparison of Papoulis-Gerchberg algorithm on USAF chart. 21
- 4.10 Mean-square error convergence of Papoulis-Gerchberg algorithm. 22

1 Introduction

As a digital microscopy project, it is inevitable that our image processing algorithms are critical for the successful implementation of our lensless design. Our team approached this task through two distinct methods: 4D light field, and limited angle tomography. Mark Hardiman and LongXiang Cui, forming NoScope's tomography sub-team, will delve into their progress and results with the iterative tomography projection method in their paper. In particular, their work deals solely with the 3D reconstruction of a microscopic sample. On the other hand, my paper will cover the entirety of light field methods, as well as the implementation of a super-resolution algorithm. In comparison to tomography, the scope of light field techniques is slightly wider; it comprises of various 2D focusing techniques on top of 3D volume reconstruction.

This paper first gives a brief overview of the concept of light-field. The next section will then cover various variations on light-field methods in order to achieve 2D digital refocusing. Following which, the paper will then move on to the 3D reconstruction algorithms which I have implemented. The final portion then elucidates the pixel super-resolution algorithm, which allows our microscope to achieve a resolution beyond the physical pixel size of our sensor.

2 Light Field Methods

The driving force behind using light field method is to allow us to digitally refocus the sample at varying depths, without the use of a lens. First described by Levoy and Hanrahan (1996) in computer graphics, the 4D light-field is a spatial and angular representation of rays of light in free-space. To be exact, we are representing light propagation as intensity in a point (in a slice of 2D space), at a given direction (described by two angles) (Levoy & Hanrahan, 1996, pg. 1), hence the four parameters.

Conventionally, light field data collection, in both photography (Ng et al., 2005), and microscopy (Levoy et al., 2006), relies on a installing a micro-lens array in front of the sensor. Each micro-lens resolves a perspective of the same scene, allowing recording of angular data of the incoming light. However, this method trades angular resolution for spatial resolution, which is especially undesirable in microscopy. In Tian, Wang, and Waller (2014)'s paper, an LED array takes over the role of the lenslet array; by illuminating the sample at a different angles one at a time, it is similar to capturing light fields of a certain oblique angle. Thus, by taking multiple exposures while switching LEDs, we are able to capture a range of 4D light field angles without sacrificing spatial resolution.

Although NoScope does not have a lens, the process and model of capturing angular data is still largely similar to that in a lensed counterpart. Figure 4.1 shows the effect of illuminating different LEDs to generate light fields of different incident angles.

Just as in Tian's work, we take sequential exposures of the sample, lighting one LED at a time. In our model, we assume that the LED's are far compared to the space between sample and sensor: the incident LED ray is thus modelled as parallel with only one angle. This forms the basis of 4D light-field collection: each image capture is a 2D intensity map, with a known incident angle (θ_x, θ_y) based on the system geometry.

The next section will explain how I used this data to perform digital refocusing using the conventional light field shift-add technique. Following which, I will propose a modified alternative to the former method.

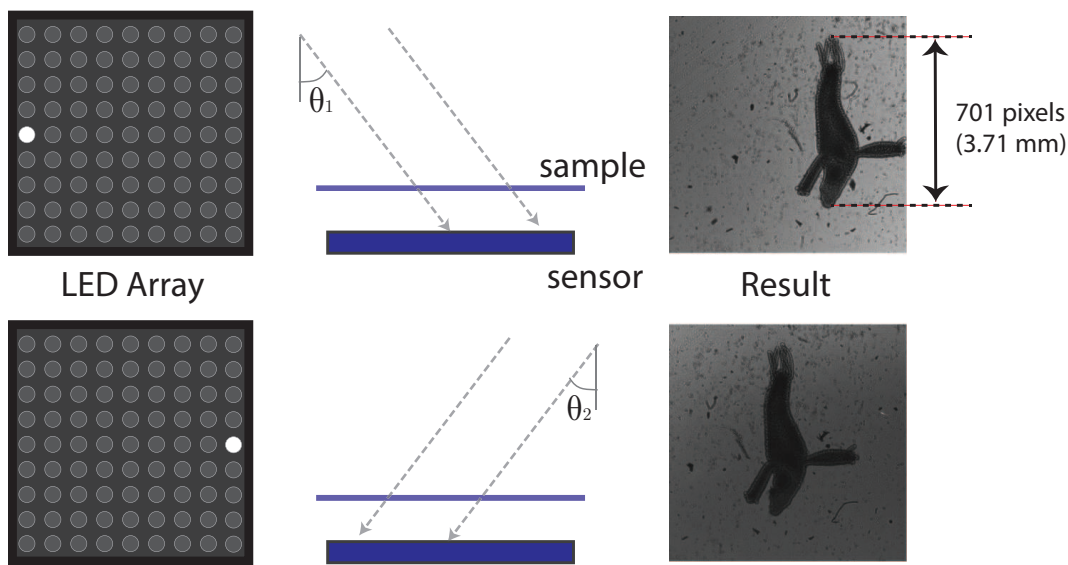


Figure 4.1: Effects of illuminating different LED. Each capture on the right is the 2D intensity map at θ_i , where i is the LED number, and θ_i the two dimensional angle of the LED normal to the sample. Note that the two images are not just translated versions of the other, but have horizontal parallax as well.

2.1 Digital Refocusing using 4D Light Field

The motivation behind digitally refocusing images from the lens-less system is to resolve depth information about the microscope sample. This will act as the foundation for 3D reconstruction, which requires knowledge of how far each feature is. Unlike the traditional microscope, the lensless setup does not have a focal plane or depth of field, and hence, we have to rely on digital refocusing to emulate depth effects instead.

Even though the hardware implementation is largely different, the working principles behind digital refocusing is still similar to that demonstrated by Ng et al. (2005, pg. 4) in photography. Strictly speaking, refocusing is an integration of the sheared 4D light field space, with the amount of shear dependent on the angle. In practice, we simply translate each image by a pre-determined amount, then sum across all images. Digital refocusing is hence synonymous with the term “shift-add”. We will derive the exact shifts in the next section.

2.1.1 Methodology – Shift-Add Implementation on Lensless setup

Assume that each LED emits a plane-wave, such that when only one LED is on, there is no angular variation across the far-field. Due to the oblique illumination, the shadow of an 3D sample will be

translated by an amount proportional to the distance to the sensor plane z , as well as the illumination angle (θ_x, θ_y) . This is a direct result of geometry, governed by $\tan\theta_x = \frac{\Delta x}{z}$, $\tan\theta_y = \frac{\Delta y}{z}$. We illustrated this in figure 4.2.

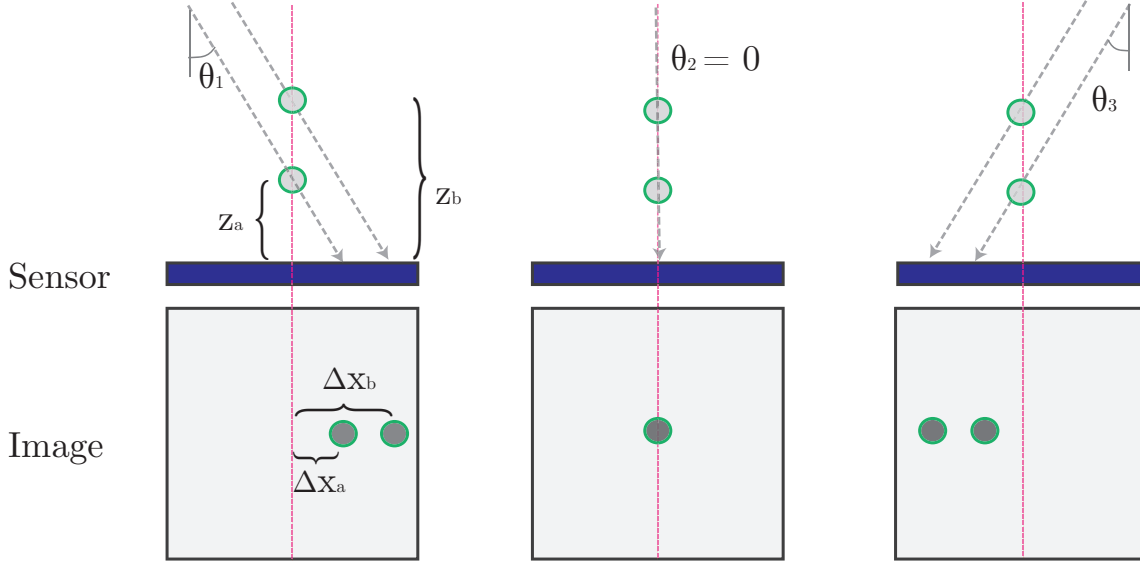


Figure 4.2: The translation of a sample in space is modeled using trigonometry. Here, we model a 3D sample as two points in space. The oblique light from LED propagates the object a distance proportional to depth. In this example, point A, of height z_a away from the sensor, is translated horizontally by $\Delta x_a = z_a \tan \theta_1$. The principle is similar for point B. Intuitively, by refocusing, we are undoing the process of oblique propagation for a specific depth.

The shift-add process eliminates effects of oblique illumination by reversing the projection process (Levoy et al., 2006). Thus, for each LED i , with angle $(\theta_{x,i}, \theta_{y,i})$, we shift its corresponding image by the amount:

$$\Delta x_i = -z \tan \theta_{x,i}, \quad \Delta y_i = -z \tan \theta_{y,i} \quad (1)$$

where z is the desired refocus depth above the sensor plane. However, we also note that $\tan\theta$ is just a function of the location of the LED on its array. We then complete the process by summing and averaging across all shifted versions.

$$F_z(x, y) = \sum_{i=1}^N I_i(x - z \tan \theta_{x,i}, y - z \tan \theta_{y,i}) \quad (2)$$

N being the number of LEDs, F_z the refocused image at depth z , and I_i the original image corresponding to LED i . In using this model for refocusing, we have assumed that light does not diffract or scatter within the sample volume, and hence will travel in a straight line.

To demonstrate digital refocusing in NoScope, we used a regular grid of 5×5 LEDs ($N = 25$) to take images of a *Drosophila* (fruit fly).

The main difference between this set up and a lensed set up is that the z -reference is taken with respect to the sensor plane, whereas with a lens, z is with respect to the focal plane.

2.1.2 Results and Discussion

Performance of Shift-Add

Figure 4.3 shows the results of digital refocusing of a *Drosophila*.

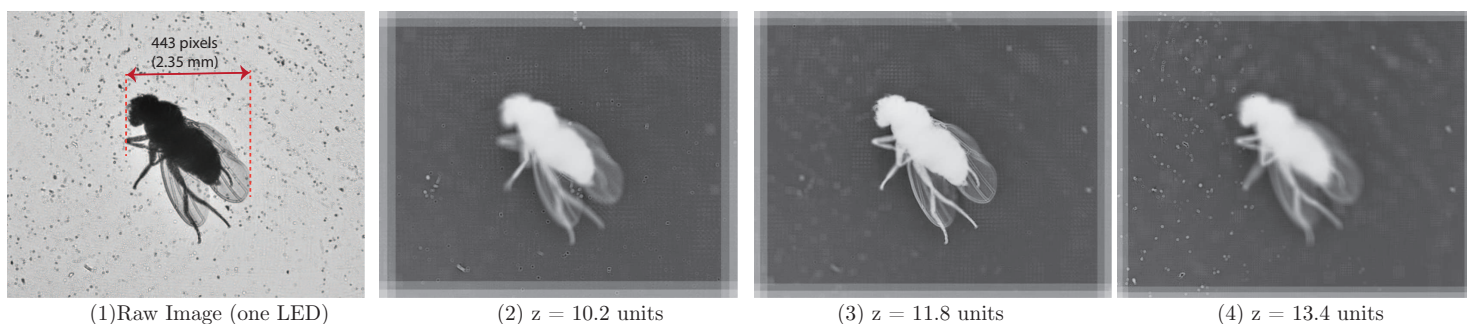


Figure 4.3: (1) shows an example of a raw image of a *Drosophila* (fruit fly) from the lens-less system. (2) - (4) shows digital refocusing at varying depth. I have processed the image in greyscale in order to reduce computational load, and also as the color channels does not give additional information in our setup. In addition, the images have been inverted for easier processing in 3D reconstruction. Refocus distance z has also been normalized in pixel distance for algorithmic simplicity.

As expected, the lensless system is successfully able to resolve the *Drosophila*, and give a out-of-focus blur for volumes that are off the digital focal plane. Note in figure 4.3, how different features appear at various depth.

One of the strong points of the shift-add algorithm is that it only requires the simple operation of shifting the original images. As such, digital refocusing can be performed rapidly ($< 0.5s$ per refocused image on MATLAB). This is crucial as the shift-add acts as the basic building block for 3D reconstruction and super-resolution later in the paper.

As for noise, the summation process bestows very good SNR performance on the refocused images. Intuitively, combining different images can be thought of as increasing the exposure time; this suppresses random photon shot noise as well as sensor noise.

Furthermore, the shift-add method is highly robust to changes in the parameters of the system.

Both sample-sensor and LED-sensor distance can be adjusted without detriment to the algorithm – we simply have to tune one parameter, the z focus distance. This lends itself to the fact that the aggregate of all translations manifest itself as a regular square grid on the cartesian coordinate; we simply have to adjust the size of the 'grid' to adapt to new parameters.

However, the shift-add generates 'grid-like' bokeh (out-of-focus blur), which is both aesthetically and practically undesirable (see figure 4.3, image (2) for example). These image artifact is a result of discrete angular sampling: the point spread function (PSF) is thus a discrete grid that spreads with depth, rather than a continuous cone. This is problematic as these gridding blends with portions of the volume which are in focus, increasing the difficult of reconstructing a 3D volume from these focal stacks.

Another subtle issue is that even with a range of z-focus distance, we have no rigorous algorithm to determine if a particular feature of the sample is in 'focus'. This meant that focus detection, especially when we are trying to initialize the system, has to be performed manually.

Resolving Power of the Lensless System

Our lensless setup's resolution is limited by two main driving forces. The first is diffraction effect. We can observe this phenomenon in all of the raw and refocused images in figure 4.3, where there are ringing patterns surrounding edges in the sample. This is a result of wave-optics leading to airy disk patterns, and obfuscates some of the finer features in the image. Unfortunately, digital refocusing does not mitigate wave-optics effect.

The second is pixel pitch. Intuitively, we can think of this as the spatial sampling frequency: the smaller the pitch, the finer we sample the spatial, the more details we can resolve. This gives a strong motivation for using smaller sub-micron pixel sizes, just like the conventional light field devices. In our current setup, we employ a camera with a pixel pitch of $5.3\mu m$, which is well above the wavelength of visible light spectrum ($< 1\mu m$). Consequently, this sets the foundation for using a much smaller pixel pitch in the next iteration of the NoScope prototype.

2.2 Localized Focusing

Despite its simplicity, the conventional shift-add algorithm falls short in the determining the depth of a sample feature. For instance, in order to focus on the middle portion of the tissue in previous example, one has to scan through a range of z focus distances, before manually selecting the z focus distance in which the feature is subjectively 'sharpest'.

In order to circumvent this issue, I proposed a modified version of the shift-add algorithm that allows quick focusing on a particular patch of the image. This concept relies on finding the maximum 'match' of a small crop of the desired feature. We do this by autocorrelating various shifted versions of the small patch with a reference image.

2.2.1 Methodology – Local Registration

The modified version of shift-add algorithm consists of the following steps:

1. Select a small patch on one LED image that we wish to focus.
2. Crop the same coordinates of the patch on images from other LEDs.
3. For each non-reference LED image extract, use a DFT correlation method (Guizar-Sicairos et al., 2008) to find the translation that gives maximum registration.
4. Use the translations from step 3 to perform shift-add.

In order to test the performance of this algorithm, we compare results of the normal light field shift-add method which gives approximately the same focus as the registration method.

2.2.2 Results and Discussion

Figure 4.4 shows the comparison of modified versus original refocusing method with two examples.

In terms of image quality, there is no perceivable difference between the normal method and the auto-correlation method. This implies that the local registration method can act as a viable alternative to quickly focus on a particular spot of the image.

One of the main advantage of using this method is that registration can be performed 'blindly'; we can throw the series of image, without knowledge of the configuration of the LEDs. More practically, we

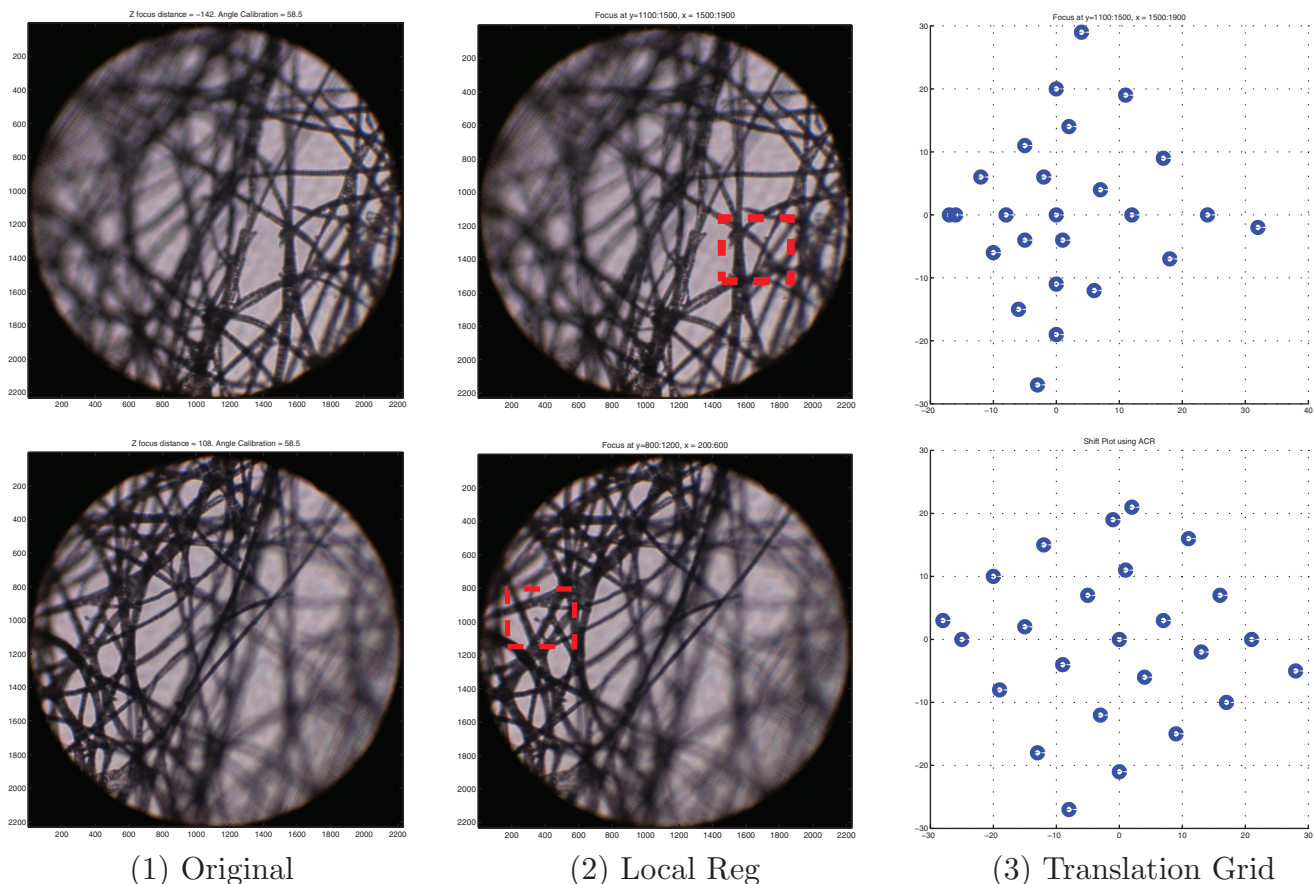


Figure 4.4: Column (1) shows the refocused image using the normal method. Column (2) shows the results from local registration. The red box shows the patch extracted for performing step 3. Column (3) shows the translations generated by autocorrelation that forms the image in (2). Each individual patch is registered with the reference patch, and its maximum translation plotted.

can use this method to calibrate our system; by using a flat target as a sample (e.g. USAF resolution chart), we can approximate the z distance of the sample holder, as well as check for any misalignment of the LED array with respect to the sensor.

In order to gain some insight into possible pitfalls of using this method, we examine the translations generated using the registration function in column (3) of figure 4.4. In the second example, the grid corresponds closely to the square grid we expect from performing regular shift-add. On the other hand, in the first example, the odd shape of the grid does suggest that this method might fail if the patch selected has volume features at multiple depths. This implies that this method of focusing is not fool-proof, and requires the assumption that the patch selected is sparse in the depth dimension.

An additional noteworthy point is that the autocorrelation algorithm we used can register up to sub-pixel accuracy (Guizar-Sicairos et al., 2008). This feature is key to motion estimation for super-

resolution, which allows us to exceed the resolution limit set by the sensor pixel pitch. We will cover this topic in the final section of the paper.

Overall, the local registration method I have proposed complements the conventional light field method; the normal method is most suitable for generating a series of image through a range of focal depth. Conversely, my method allows users to target a specific feature within the sample directly, but generating only one refocused image at a time.

3 3D Reconstruction

Our team strongly believes that 3D imaging is the new paradigm of microscopy. By visualizing samples in three dimensions, the hologram can reveal inherent structures that would otherwise have been hidden in a normal microscope image.

The previous section on light-field refocusing is concerned with generating stacks of 2D images at different focal depths. Those results were vital to moving into 3D imaging, one of the key value propositions of NoScope. This section builds upon the results of those image stack to reconstruct a 3D volume representation of the microscopic sample.

In approaching this problem, I have adopted two distinct methods. The first is a more mathematically rigorous, well-researched, but slower technique of 3D deconvolution. The second is a 'hack' I devised in order to achieve 3D reconstruction with little computation, but lacks the accuracy of the first. This section will explain and examine the results of both methods, and make a comparison, as well as a recommendation of which technique users should use.

3.1 3D Deconvolution

3D deconvolution attempts to construct a 3D volume by solving an inverse problem from the stack of digitally refocused image. Intuitively, based on our model used for digital refocusing in the previous section, each voxel (point in 3D volume) will have a point spread function (PSF) of a grid-like structure that spreads with depth. By 'tracing' the spread of these grid lines, we are essentially solving for the depth in which each voxel exist, hence giving us a 3D structure.

Broxton et al. (2013, p.8) has previously demonstrated this technique in conventional light field microscopy. However, since our setup has no lens, formulating the model takes a slightly different route. In particular, the forward model – describing the one-way relation of voxel to refocused images – takes a different tack, and is fact slightly simpler due to the lensless set up.

3.1.1 Projection Model and Lucy-Richardson Algorithm

We formulate the problem as such: given the stack of digitally refocused image f , invert the following forward model:

$$f = Hg \quad (1)$$

$$g = \begin{bmatrix} g_1 \\ g_2 \\ \vdots \\ g_n \end{bmatrix}, \text{ where } g_i \text{ is a plane of } r \times c \text{ voxels, } g \text{ forming the entire volume} \quad (2)$$

$$f = \begin{bmatrix} f_1 \\ f_2 \\ \vdots \\ f_n \end{bmatrix}, \text{ where } f_i \text{ the } i^{\text{th}} \text{ inverted acquired image of } r \times c \text{ pixels} \quad (3)$$

$$H = \begin{bmatrix} H_{1 \rightarrow 1} & H_{2 \rightarrow 1} & \dots & H_{n \rightarrow 1} \\ H_{1 \rightarrow 2} & H_{2 \rightarrow 2} & \dots & H_{n \rightarrow 2} \\ \vdots & & \dots & \vdots \\ H_{1 \rightarrow n} & H_{2 \rightarrow n} & \dots & H_{n \rightarrow n} \end{bmatrix}, \text{ where } H_{i \rightarrow j} \text{ is the convolution operator of } g_i \text{ to part of } f_j. \quad (4)$$

This is the same formulation used in Broxton's (2013) paper, but the similarity ends here. In our model, the projection of each layer of voxels (g_i) to each acquired image (f_j), described by the operator $H_{i \rightarrow j}$ is simply given by a translation, $\Delta x = z_i \tan \theta_{x,j}$, $\Delta y = z_i \tan \theta_{y,j}$. θ_j refers to the incident angle of the j^{th} LED. Likewise in the digital refocusing section, we are taking the first Born approximation (Born & Wolf, 2000) with the ray optics model, assuming no scattering within the 3D sample and ignoring phase effects.

Note that the translation amount corresponds to the exact opposite of digital refocusing — the forward problem is simply the reverse process of digital refocusing. This gives us a convenient formulation for setting up the problem: we can digitally refocus the specimen at arbitrary depths, then pass on the shift parameters for generating the focal stack to the deconvolution algorithm. The forward model can thus utilize the same set of parameters to project g to f .

Formulating the 3D reconstruction problem in such a manner gives us a hint to the depth resolution of the final 3D model. g is rank limited by the number of raw images we acquire in f , and it seems intuitive that we should only be able to resolve an amount of voxel layers no more than the number of base images we have.

Unfortunately, the inverse problem is ill-conditioned, and an exact solution most often do not exist, due contribution of random sensor noise and slight numerical inaccuracies of our model. Therefore, we rely on an well-known iterative method known as Lucy-Richardson deconvolution (Lucy, 1974; Richardson, 1972) to solve for g .

$$g^{k+1} = (H^T \frac{f}{Hg^k}) \cdot * g^k \quad (5)$$

where H refers to the forward projection described above, while H^T is the backward projection model. All division and multiplication are element-wise operations. Conveniently, we already possess the necessary tools for performing this iterative method – the backward projection is simply the digital refocusing process.

The reason for choosing the Lucy-Richardson method is that this algorithm is robust, and will likely converge given enough iterations. In addition, since this is a well-established deconvolution method, many modifications exist to optimize the noise-tolerance and convergence rate of the algorithm.

Acceleration and Regularization of LR Algorithm

The vanilla LR algorithm suffers from several weakness. First, the algorithm is nonlinear, and hence may take a large number of iterations before converging. Second, direct division in the deconvolution process ($\frac{f}{Hg}$) can be unstable as there might be 0 pixel values after each forward projection.

To address the first issue, I used an accelerated version of the LR algorithm by placing an exponent factor p_k in the correction term on each iteration. A larger exponent increases step size, and hence convergence speed, but at the sacrifice of stability, and vice versa. Hence, by putting a larger step size initially, and rapidly pushing it down for later iterations, we can obtain both faster convergence and stable result. A value of $p = 3$ is empirically known to be acceptable for an initial step size (Singh et al., 2008), before tapering it to $p = 1$ at the end. As for the instability due to division, I added a

regularization constant λ after the forward projection. The final algorithm I implemented is thus:

$$g^{k+1} = \left(H^T \frac{f}{Hg^k + \lambda} \right)^{p_k} * g^k \quad (6)$$

3.1.2 Methodology

In order to validate the deconvolution method, I used a Shepp-Logan 3D phantom model of size 128x128x32 to simulate its own digitally refocused images using the forward model I proposed above. I used a 5x5 grid to simulate the projections from a grid of LEDs. Following which, I employed the Lucy-Richardson method to recover the 3D phantom, before comparing the results against the original model at various numbers of iterations.

Following which, I implemented the algorithm on a series of actual microscopic specimens obtained from NoScope, using a grid of 5x5 LEDs around the center.

Following, I examined the convergence rate of the algorithm by calculating a mean-square-error difference of the reconstruction with its previous iteration, and make a recommendation for number of iterations.

3.1.3 Results and Discussion

Simulation

Figure 4.5 shows a comparison of the 3D phantom with its original, ending at various number of iterations.

The deconvolution process is largely able to reconstruct phantom model, retaining major shapes and features. However, this reconstruction method introduces undesired ringing artifacts; this is a well-known drawback of using the Lucy-Richardson algorithm. The ringing artifacts increases with number of iteration, but at the same time, we require an acceptable amount of iteration for the deconvolution to converge. Thus, there is a trade-off with the number of iterations. Empirically, from this simulation, I determine a rule of thumb of 10-20 iterations to be optimal.

Another issue to contend with is the speed of the algorithm. Even though we are using a volume with relative low voxel count, each iteration already takes more than 3 seconds to run. Furthermore,

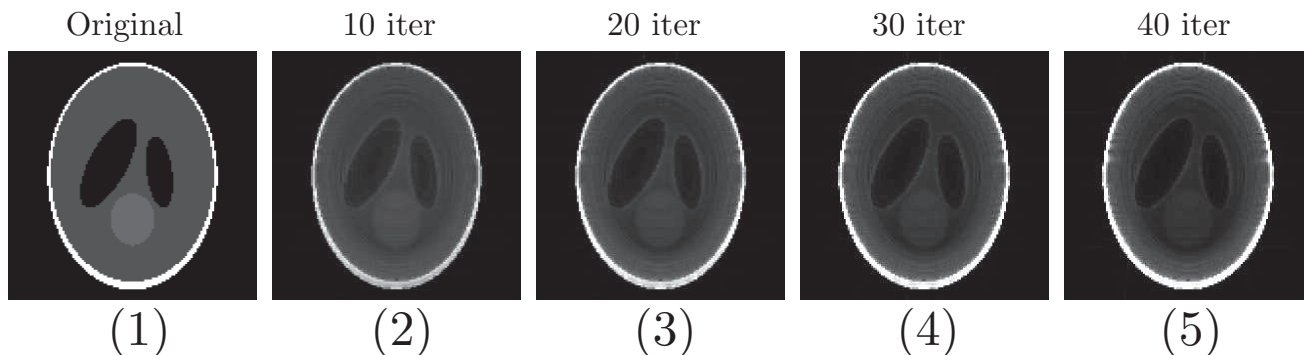


Figure 4.5: (1) is the original slice from the phantom. (2) is after 10 iterations, etc. Note that the ringing noise increases with number of iteration, and the reconstructed slice gradually loses energy. This is clearly undesirable, and we aim to cut the iterative process as early as possible without sacrificing convergence.

the computational complexity scales with approximately the squared of the number of voxels; this is due to the nature of the H operator. Practically, this means each iteration with the actual lensless microscope sample can take up to half a minute to run, and the whole deconvolution up to the order of half an hour. For a user desiring quick visualization of a 3D structure, the time required may make deconvolution impractical.

On a more optimistic note, the deconvolution can benefit greatly from several optimization steps. The first is parallelization; the deconvolution algorithm comprises mostly of shift-adds, which can be easily split into multiple threads for a significant speed up. We can obtain even further speed increase by deconvoluting a GPU array instead. The second is that the most computationally-heavy process is the image translation in the forward and backwards model. There are many alternatives for performing sub-pixel translations (such as fourier phase ramps), thus improving the runtime of the algorithm.

Actual Samples

Figure 4.6 shows the 3D reconstruction from actual samples acquired from the lensless setup.

In general, the LR algorithm is able to pick out depth structures of the specimens that would otherwise have been unobservable from the raw 2D images. The algorithm is robust across a variety of microscopic samples, without much need for tuning.

An issue to contend with is the fact that the illumination does not have enough intensity to penetrate the body of the samples. For instance, in the cockroach head, most of the head of the body remains black. This gives the algorithm difficulty in resolving the insides of specimens. This also gives a

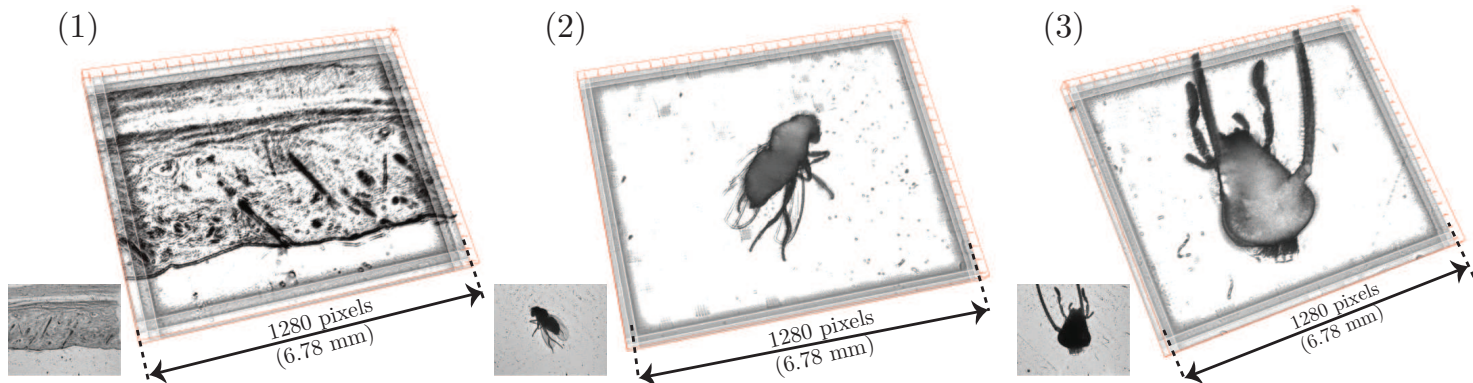


Figure 4.6: (1) - Human hair follicle. (2) - *Drosophila* (fruit fly). (3) - Cockroach head. All three are performed with 20 iterations of the accelerated, regularized, LR algorithm, 5X5 LEDs. 3D structure represented using Fiji 3D viewer, with no thresholding, and no post-processing on images after deconvolution.

motivating factor for placing the LED array much closer to the sensor.

Moreover, aside from the run time of the algorithm (approximately 1 hour for each 3D reconstruction), we run into practical issues regarding memory. The deconvolution is a memory intensive process, and unless the images are down-sampled, a 25 layered image stack is the practical limit in which we can perform deconvolution on. This currently puts a constrain on the number of images we can work with, and consequently, the depth resolution of the 3D sample.

3.2 An Novel Alternative: Hacking the 3D reconstruction

A clear weakness of the 3D deconvolution algorithm is that it simply takes too long to run. This is especially problematic for NoScope, since we envisioned our users to be mainly medical professionals on the field, with little computational power at their fingertip. For 3D imaging to be practical, we need an algorithm that can run more efficiently on a lean setup.

With this background in mind, I propose a image processing 'hack' to achieve 3D imaging quickly and efficiently. This technique is inspired by how a modern digital camera detects focus: by scanning through a range of focal distance, it settles on a configuration that yields maximum contrast. Similarly, by running our refocused images through a series of filters, we extract portions of the focal stack that have edges and sharp features, and hence are 'in focus'. Following which, I stacked the extracted features to form a 3D volume.

3.2.1 Methodology – Focus Estimation and Extraction

We begin from the stack of refocused images from the shift-add algorithm. In order to detect if a particular feature in an image is in focus, I filtered the images using the Sobel filter. This kernel acts as a edge detector, and consequently produces greyscale images of the sharpest feature within in each. This is the approximation to 'focus', where I assumed that features in focus will have sharp edges and higher contrast. Conversely, portions of the image blurred by the grid-bokeh will be discarded by the filter.

The second step producing a mask from the edge detection images in step 1. The purpose of the mask is to approximate a region in which the image is in focus. I used a Gaussian low-pass filter over the images in step 1. Intuitively, this smears the thin edges we extracted in step 1, giving an approximation to focused area. I then threshold the low-pass edge images to produce the mask.

The third step is to invert the original focal stack in greyscale, and apply the mask over those image. The image mask effectively zeros the unfocused regions, while retaining area where there is high contrast. This approximates the depth in which the feature exist within the volume, hence giving us our low pass image. This process is summarised in figure 4.7.

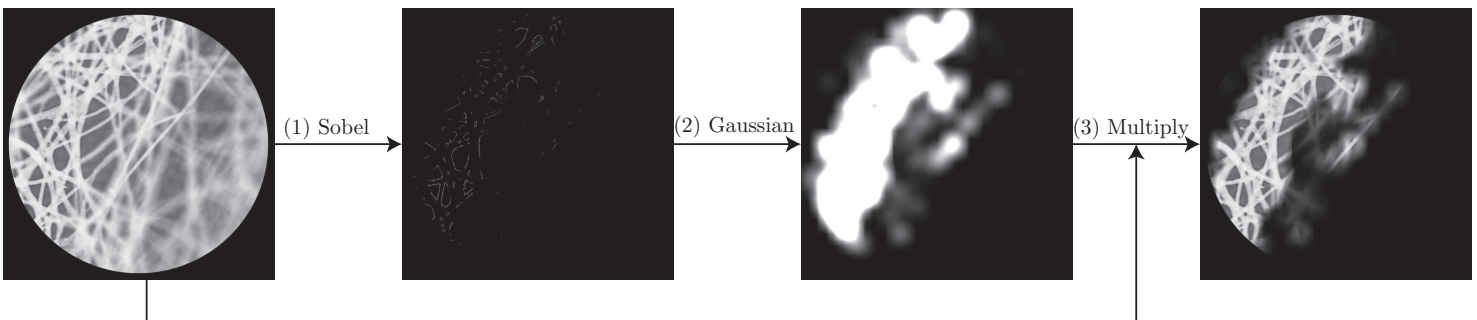


Figure 4.7: An example of the focus extraction process flow-chart for one layer of the focus stack. (A)

There is flexibility in choosing the two filters used in the processing. Strictly speaking, any high-pass filter can replace the Sobel operator, and low-pass, the Gaussian. In this case, I chose the Sobel operator as it is extremely fast to compute (the kernel is only 3x3 pixels), while other larger filters slows computation without better performance.

As for the Gaussian, it has the nice property of being circularly symmetric, and also a pleasing fade at its tail. This makes the mask appear more natural, as opposed to low-pass filters like a block-

average, which yields blocky artifacts in the focus region approximation. Furthermore, since the Gaussian is 2D-symmetric, we can perform the 2D filter via a sequential 1D Gaussian filter. This speeds up computational time significantly. Overall, the Gaussian kernel gives a good compromise between aesthetics and performance.

3.2.2 Implementation and Discussion

Figure 4.8 shows some examples of implementation on microscopic samples.

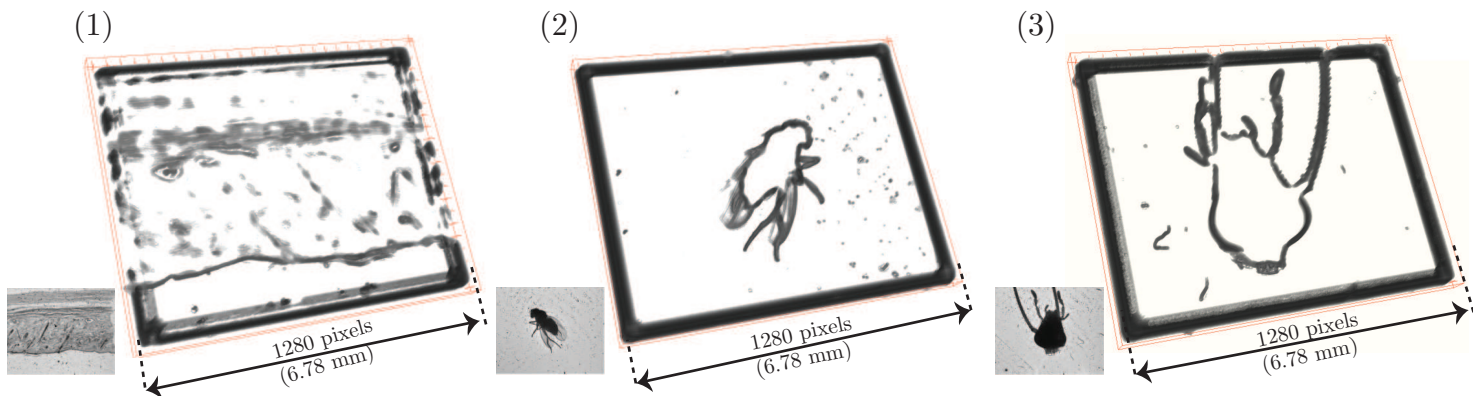


Figure 4.8: (1) - Human hair follicle. (2) - *Drosophila* (fruit fly). (3) - Cockroach head, just as in 3D deconvolution. Notice the empty spaces within large volume chunks. As before, no post-processing and thresholding were applied to the image stack for 3D visualization.

The algorithm is able to extract features at different depths very quickly, allowing us to reconstruct a 3D volume of the sample. As the process consists entirely of a series of filters, we are able to compute the 3D volume in the order of seconds. Undeniably, this method is much faster than the 3D deconvolution method in the previous section.

Aside from being fast, this algorithm holds the advantage of being easy and intuitive to fine-tune. The only two main parameters to tweak are the strength of the Sobel and the length of the Gaussian filter. Tuning the Sobel can be viewed as choosing a cut-off contrast level, in which the algorithm will detect as being 'in focus'. Similarly, increasing the strength of the Gaussian filter increases the 'smear' of the edge detection, allowing more area to be included in the mask.

Furthermore, the choice of filters in processing is not restrictive: users can plug in different filters if desired to extract the type of focal features within the object. This opens up the option of customization for NoScope users.

However, this hack for reconstructing 3D volume has two limitations. The first the algorithm cannot

pick out objects with low contrast. Objects too far away from the sensor may lose sharpness due to the spread of light. These blurred features do not generate enough contrast, and consequently, the Sobel filter might not be able to pick out these regions as being in focus. Naturally, this leads to small pockets of empty spaces in the 3D reconstruction. The missing segment in the fruit fly's wing in figure 4.8 (Sample (2)) illustrates this effect.

The second weakness is that edge-based focus detection meant that large volume reconstruction may be inaccurate. The areas which the algorithm selects as focused is governed by the edge detection filter. For large volumes with no distinct features within, the Sobel filter will not detect any edges inside, and the reconstruction manifests as a shell rather than a filled object. An example of this is image (3) in figure 4.8, where the dark shadow of the cockroach head appears as a empty shell in the reconstruction, whereas in 3D deconvolution, the algorithm reconstructs it as a full volume.

3.2.3 Comparison with 3D Deconvolution

Nonetheless, despite its shortfalls, the method I proposed remains useful as a quick alternative to the 3D deconvolution method. For microscopic samples that do not possess a large volume feature relative to the field of view, the filter method is quick, robust, and accurate enough to discern the underlying 3D structure of the sample. However, if time and efficiency is not of the essence, then the original 3D deconvolution method should be the recommended method; its reconstruction is less feature sensitive, allowing higher volume fidelity across different samples.

Overall, the two methods complement each other in giving users of NoScope the choice of choosing between an 3D algorithm that is fast and efficient, or another that is slower, but more accurate. In putting the algorithm in NoScope, my recommendation is to first run the hack method to quickly obtain a 3D structure without much computation, then giving users the option to 'increase accuracy' by performing 3D deconvolution in the background.

4 Pixel Super-resolution

While the previous sections presented methods of refocusing and reconstructing volume, this section will move on to the different topic of improving our resolution, the fundamental driving force behind NoScope as a microscope.

Unlike a conventional microscope which uses lenses to magnify samples, NoScope relies entirely on the small size of modern camera sensors to give a desired magnification. The smaller the pixel pitch on our sensor, the more details NoScope will be able to resolve. Thus, the seeming innocuous way of improving resolution is to simply buy sensors with very small pixels.

However, purchasing sensors with very small pixel pitch, while having a larger field of view (e.g. APS-C sensors in DSLR), can be expensive. Furthermore, the smaller the pixel size, the poorer its light collection ability. This drives up photon shot noise, complicating post-processing. This drives the motivation for finding a method to increase our resolution beyond the inherent limit set by the physical pixel on the sensor.

With this context in mind, the field of super-resolution (SR) naturally emerged as the solution. The basic idea behind super-resolution is that we take several sub-pixel shifted, low resolution images of the same scene, combine them with signal processing techniques, and form a high resolution image (Park et al., 2003, pg. 2). The resulting high resolution image is known as a super-resolution reconstruction.

Lens-less super-resolution has been previously achieved by Isikman (2011), where an electronically actuated optic fibre is jittered. This fibre, when coupled to a light source, gives rise to sub-pixel shifted images for SR processing (Isikman et al., 2011, pg. 2). In our case, we obtain the low-resolution image differently by moving the sensor itself instead of the light source; we mount the sensor on a two-directional moving stage. We then manually translate the stage by a random amount while taking images of the same scene on one LED.

A description of the hardware for achieving this portion can be found in Ying Ou's technical paper. Instead, this section, will present the signal processing algorithm I used to obtain super-resolution after taking those translated images.

4.1 Methodology - Papoulis-Gerchberg Algorithm

The first step for SR processing is to estimate the motion between the randomly translated raw images. Our setup restricts the sensor to move in a plane, while maintaining its orientation. This means that the raw images will just have pure translations and no rotation components. This is fortunate for us, since we already employ an efficient registration algorithm in the section on localised focusing. This DFT registration method allows motion-estimation up to sub-pixel accuracy efficiently (Guizar-Sicairos et al., 2008).

From the motion estimation parameters, we now have a range of choice between existing super-resolution algorithms. The method I chose is a projection onto convex sets approach known as the Papoulis-Gerchberg (PG) method (Gerchberg, 1974). The reason for choosing this algorithm is that it is relatively easy to implement. Furthermore, despite requiring many iterations to converge to a solution, the most complex operation is the FFT, which is a highly optimized algorithm on MATLAB.

The PG method is as such: first, fit values of the low resolution image on a desired high resolution grid. Use zeros for pixels which does not have any data. Second, perform a FFT on the high resolution grid. Third, zero the high frequency components of the DFT by using a rectangle window. Fourth, transform back to the spatial domain via IDFT. Lastly, reinforce data consistency restoring known pixel values from the low resolution image to their actual value. This process is then iterated, until a desired MSE is reached.

Unfortunately, this method is well know for its sluggish convergence, and requires many iterations before arriving at a satisfactory image (Salerno, 1998, pg. 7). Furthermore, choosing the low-pass cut off frequency takes some guesswork, and may require prior knowledge about the type of image we are taking.

This gives the motivation for further improving the algorithm. I used a modification proposed by Salari and Bao (2012), where we pre-process the high-resolution grid before iteration. The first step involves interpolating the zero values by averaging the non-zero values around it. This fills the void in the initial grid. Second, we adaptively adjust the low-pass cutoff frequency with each iteration, based on the iteration MSE. The idea is that we start off with a low cut-off frequency to increase convergence rate, and subsequently decreasing the strength of the cut-off so we still can arrive at a solution with

high-frequency details.

I tested the super-resolution algorithm on our lensless setup by taking images of a USAF resolution target chart, and performing a 4x resolution increase using both methods. Further on, I will make a comparison of the modified PG algorithm versus the original version. Lastly, I will characterize the resolving power of NoScope using the USAF line-pair standards.

4.1.1 Results and Discussion

Performance of SR Image

The original PG method converged in 61 iterations, while the modified version, in 48. Figure 4.9 shows the results from the two method.

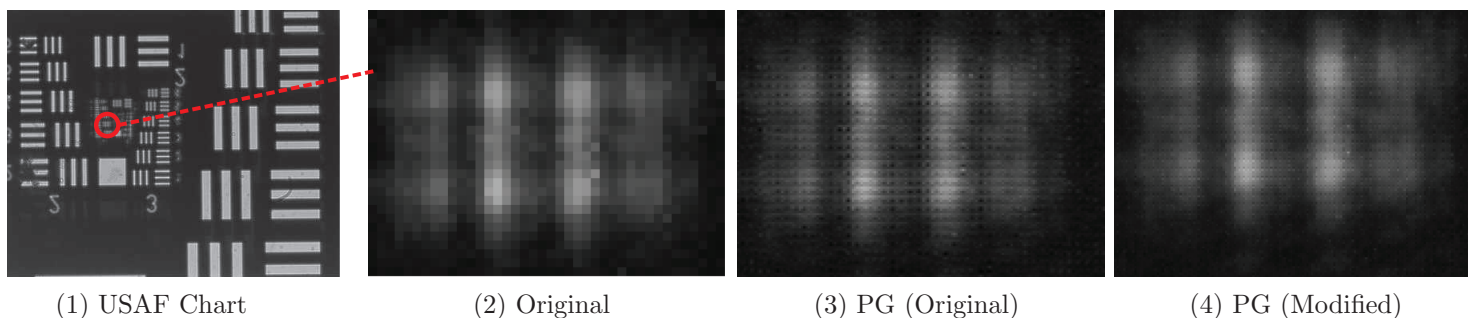


Figure 4.9: (1) shows the entire USAF chart. (2)-(4) zooms in on one set of line pair using different methods. (2) is the normal method. (3) is the original PG method (4x), with 61 iterations. (4) is the modified PG method (4x), with 48 iterations. The convergence criteria is if overall MSE is less than 10^{-2}

The result from the modified algorithm, arguably, is more aesthetically pleasing. The original algorithm produces pixelation artifacts even at convergence. On the other hand, the modified PG method is much smoother, due to the initial interpolation step. In both cases, we have successfully increased the resolution beyond that allowed by the physical pixel size.

Characterizing the exact resolving power is a subjective process, and is dependent on what the user deems as acceptable contrast. In our case, with super-resolution, we are able to view the group 5, element 1 line-pair with medium contrast. This corresponds to a resolving power of 32 line pair/mm. In contrast, we are only able to view the same line pair in the original image with lower contrast, with only a single pixel resolution.

A limiting factor of purely using the PG method is that the algorithm does not overcome the effects

of diffraction, the main source of blur in NoScope’s images. This opens up a scope for future work in subsequent iterations of NoScope; using a forward model with diffraction in wave theory, we can further deconvolve our image to obtain higher resolution.

Algorithm Convergence Rate

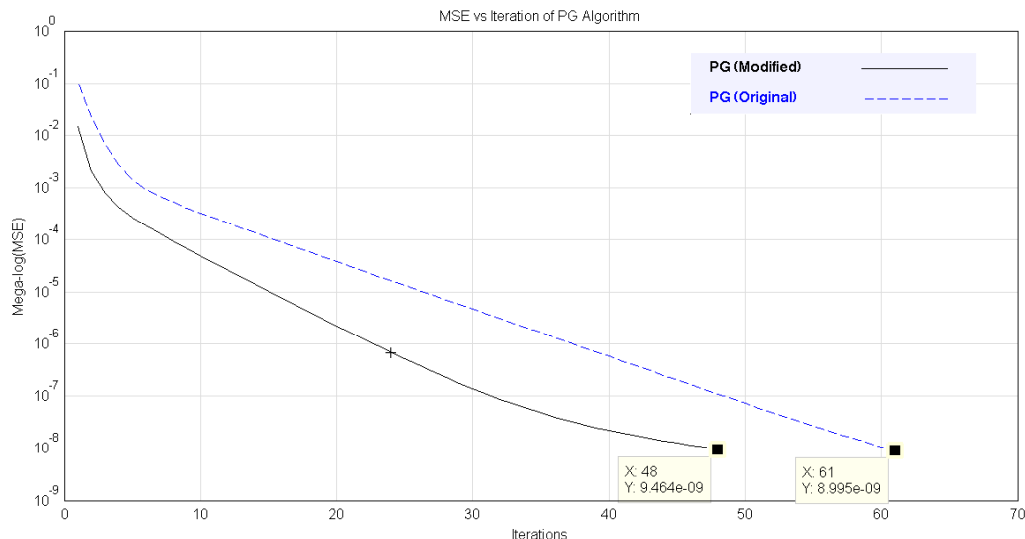


Figure 4.10: Convergence rate of the original PG algorithm, vs the modified version. The MSE cut-off is 10^{-2} .

In addition, the convergence time of the modified algorithm is evidently superior to that of the original, as shown in figure 4.10. At all iterations, the modified version gave a lower MSE per iteration. With both improved convergence rate, and visually smoother output, the modified algorithm is undeniably better, and hence will be used as the final image processing algorithm.

Another noteworthy issue we should examine is the number of images required to form a super-resolution image. In terms of processing, we can intuitively see that too few images gives the PG algorithm too little information to start with. Conversely, if too many raw images are taken, the additional images yield diminishing information. Moreover, since we are shifting the sensor manually in our setup, taking more images will require more time. Generally, I found that using 8 images for a 4x reconstruction is fairly optimal, and taking more images yields little additional information.

Aside, I have also found that it is impractical to push the SR algorithm beyond 4x, due to memory constraints. An 6x or 8x PG algorithm uses up too much memory for a typical laptop to handle, often resulting in software crashes. A possible investigation for future work is to optimize the memory

allocation of the PG algorithm to run on systems with 4GB to 8GB of RAM.

Further Work

A natural question to ask is if the super-resolution work presented in this section can be used as the basis for images in both 2D digital refocusing, and 3D reconstruction in light field and tomography. Theoretically, the results we have show that we can easily extend the results of one SR image to multiple SR images taken with different LEDs. However, in our current iteration of hardware, the translation of stage is done manually. If we were to use a 5x5 grid like those in the light field refocus section, this would correspond to a total of 200 images in total, assuming 8 raw images per SR image. Data collection would undoubtedly be a laborious process.

Having said that, this provides motivation for automating the moving stage in our next iteration of the lensless set up. This could perhaps be done by incorporate a small actuator into the knob of the moving stage, and integrating the control with our Arduino.

Another major limitation in increasing resolution is the diffraction effect. As we put the pixel pitches close to sub-micron levels, we will undoubtedly observe wave optics effect on our images. Modelling, and deconvoluting the effects of these patterns will be key to improving the resolution.

5 Conclusion

In this paper, I have presented the light field methods for digital refocusing and 3D reconstruction for the software side of our microscope. I performed digital refocusing using the light field method, and proposed a modified algorithm to allow for localised focusing. In both cases, the algorithm is very robust to changes in hardware parameters, and computationally efficient. The 2D refocused images forms the basis for 3D reconstruction.

Following which, I presented two distinct volume reconstruction methods. The first is a well-research, conventional method of 3D deconvolution. The alternative is a clever hack that employs a series of filters to estimate the structure of a 3D sample. This two methods complement one another by giving NoScope users the choice of trade-off between speed and accuracy.

Lastly, I delved into the topic of super-resolution, that allows NoScope to increase its resolving power beyond that of the physical pixel size. I explored a form of POCS algorithm known as Papoulis-Gerchberg method, at the same time modifying it for faster convergence. This SR method increased the resolution of NoScope at little cost, pushing us closer to our goal of making NoScope a viable medical diagnosis device.

References

- Born, M., & Wolf, E. (2000). *Principles of Optics: Electromagnetic Theory of Propagation, Interference and Diffraction of Light*. CUP Archive.
- Broxton, M., Grosenick, L., Yang, S., Cohen, N., Andalman, A., Deisseroth, K., et al. (2013, October). Wave optics theory and 3-D deconvolution for the light field microscope. *Optics Express*, *21*(21), 25418–25439. Available from <http://www.opticsexpress.org/abstract.cfm?URI=oe-21-21-25418>
- Gerchberg, R. (1974, September). Super-resolution through Error Energy Reduction. *Optica Acta: International Journal of Optics*, *21*(9), 709–720. Available from <http://dx.doi.org/10.1080/713818946>
- Guizar-Sicairos, M., Thurman, S. T., & Fienup, J. R. (2008, January). Efficient sub-pixel image registration algorithms. *Optics Letters*, *33*(2), 156–158. Available from <http://ol.osa.org/abstract.cfm?URI=ol-33-2-156>
- Isikman, S., Bishara, W., Sikora, U., Yaglidere, O., & Ozcan, A. (2011, November). Multi-angle illumination with pixel super-resolution enables lensfree on-chip tomography. *SPIE Newsroom*. Available from <http://www.spie.org/x84293.xml>
- Levoy, M., & Hanrahan, P. (1996). Light Field Rendering. In *Proceedings of the 23rd Annual Conference on Computer Graphics and Interactive Techniques* (pp. 31–42). New York, NY, USA: ACM. Available from <http://doi.acm.org/10.1145/237170.237199>
- Levoy, M., Ng, R., Adams, A., Footer, M., & Horowitz, M. (2006). Light Field Microscopy. In *ACM SIGGRAPH 2006 Papers* (pp. 924–934). New York, NY, USA: ACM. Available from <http://doi.acm.org/10.1145/1179352.1141976>
- Lucy, L. B. (1974). An iterative technique for the rectification of observed distributions. *The Astronomical Journal*, *79*, 745.

- Ng, R., Levoy, M., Brédif, M., Duval, G., Horowitz, M., & Hanrahan, P. (2005, April). *Light Field Photography with a Hand-Held Plenoptic Camera* (Tech. Rep. No. 2005-02). Palo Alto, CA, USA: Stanford. Available from <http://hci.stanford.edu/cstr/reports/2005-02.pdf>
- Park, S. C., Park, M. K., & Kang, M. G. (2003, May). Super-resolution image reconstruction: a technical overview. *IEEE Signal Processing Magazine*, 20(3), 21–36.
- Richardson, W. H. (1972, January). Bayesian-Based Iterative Method of Image Restoration. *Journal of the Optical Society of America*, 62(1), 55–59. Available from <http://www.opticsinfobase.org/abstract.cfm?URI=josa-62-1-55>
- Salari, E., & Bao, G. (2012, October). Super-resolution using an enhanced Papoulis-Gerchberg algorithm. *IET Image Processing*, 6(7), 959–965.
- Salerno, E. (1998). Superresolution capabilities of the Gerchberg method in the band-pass case: An eigenvalue analysis. *International Journal of Imaging Systems and Technology - INT J IMAGING SYST TECHNOL*, 9(23), 181–188.
- Singh, M. K., Tiwary, U. S., & Kim, Y.-H. (2008, January). An Adaptively Accelerated Lucy-Richardson Method for Image Deblurring. *EURASIP J. Adv. Signal Process*, 2008, 52:1–52:10. Available from <http://dx.doi.org/10.1155/2008/365021>
- Tian, L., Wang, J., & Waller, L. (2014, March). 3d differential phase-contrast microscopy with computational illumination using an LED array. *Optics Letters*, 39(5), 1326–1329. Available from <http://ol.osa.org/abstract.cfm?URI=ol-39-5-1326>

Part V

Concluding Reflections

1 Concluding Reflections

In using light-field processing, I have been able to achieve most of the initial objectives early last semester, namely 2D digital refocusing, and 3D reconstruction, using the focus extraction method. In addition, the actual codes we had to write were greatly simplified as the team decided to shift our focus away from a standalone embedded system to one attached to a laptop; we did not have to write specialized embedded code for processing. As such, the set of algorithm I implemented has been a safety net for the software side of our capstone team, giving the tomography team breathing space to explore the limited angle method for an alternate method for 3D reconstruction. Similarly, for myself, I had room to explore topics that were not initially planned, such as super-resolution, and 3D deconvolution. Consequently, we were able to expand the number of features and functions NoScope has, on the image-processing side.

In terms of project management, the most important takeaway is that for projects that involves major learning tasks, the team must be adaptive with the project plan, and be open to re-evaluating project goals at regular intervals of the project. In the capstone, we had a tricky balance of managing a project that is both academic and product-oriented at the same time. Furthermore, all of us were uninitiated in the fields of light-field and tomography in the beginning, and our capstone team grossly underestimated the amount of time required for learning tasks. For instance, even though we initially allocated one month for the tomography team to learn about limited-angle tomography, the team was clearly far from learning enough to implement an algorithm on NoScope. This is simply due to the open-ended nature of the task. Evidently, it was more important that we were able to take stock of our own progress during team-meetings, and adjust our goals accordingly.

Undeniably, there is still much work to be done for NoScope to become a truly cheap and portable microscope. On the light-field side, I have focused on achieving a wide breadth of functionality for the microscope. As such, my work can serve as a groundwork for deeper investigation. For 3D deconvolution, one can still explore TV regularization for edge-preservation, as well optimize number of iterations and acceleration step for reducing computational time. For super-resolution, further extend the super-resolution model by including a deconvolution process that accounts for wave optics: this is critical for our vision of eventually imaging malaria cells, which are in the order of sub-microns.

On the hardware side, I believe that are two key objectives that NoScope needs to achieve. The first is reducing pixel pitch. Our current prototype uses a ($5.3\mu\text{m}$) pixel pitch, which still has much more room for improvement. Naturally, a reduction in pixel pitch must run in tandem with processing algorithms that account for wave effects, especially as we approach the diffraction limit. In addition, the next focus is also on miniaturization. As of now, NoScope is still cumbersome, and more fragile than we envision it to be. My recommendation is to include a product designer in the following NoScope team who can specialize solely on this task.